Chemistry Europe
European Chemical Societies Publishing

WILEY VCH

Excellence in Chemistry Research

Announcing our new flagship journal

- Gold Open Access
- Publishing charges waived
- Preprints welcome
- Edited by active scientists

Meet the Editors of *ChemistryEurope*

Luisa De Cola
Università degli Studi di Milano Statale, Italy

Ive Hermans
University of Wisconsin-Madison, USA

Ken Tanaka
Tokyo Institute of Technology, Japan

ChemCatChem

The European Society Journal for Catalysis

Chemistry Europe

European Chemical Societies Publishing

Supported by

GECATS GERMAN CATALYSIS SOCIETY

Accepted Article

Title: Small Angle Scattering Techniques for the Study of Catalysts and Catalytic Processes

Authors: Facundo Herrera, Gonzalo Rumi, Paula Y. Steinberg, Alejandro Wolosiuk, and Paula Cecilia Angelomé

To be cited as: *ChemCatChem* **2023**, e202300490

Link to VoR: https://doi.org/10.1002/cctc.202300490

WILEY VCH

Small Angle Scattering Techniques for the Study of Catalysts and Catalytic Processes

Dr. Facundo Herrera[1#], Dr. Gonzalo Rumi[1#], Dr. Paula Y. Steinberg[1,2#], Dr. Alejandro Wolosiuk[2,3*], Dr. Paula C. Angelomé[2,3*]

(1) Laboratorio Argentino de Haces de Neutrones, CNEA, Av. General Paz 1499, 1650, San Martín, Buenos Aires, Argentina
(2) Gerencia Química, CAC, CNEA, Av. General Paz 1499, 1650, San Martín, Buenos Aires, Argentina
(3) Instituto de Nanociencia y Nanotecnología, CONICET, CAC, CNEA, Av. General Paz 1499, 1650, San Martín, Buenos Aires, Argentina

[#] These authors contributed equally to this work.
* Corresponding authors, emails: wolosiuk@cnea.gov.ar (A.W.) & angelome@cnea.gov.ar (P.C.A.) Webpage: www.qnano.com.ar (A.W. & P.C.A.)

Abstract

Small-Angle Scattering (SAS) techniques are essential tools for the characterization of catalysts before, during and after catalytic reactions. Either based on X-Rays (SAXS) or neutrons (SANS), they provide unique structural information that helps to understand catalytic processes at the nanoscale level, allowing a rational improvement of the catalysts design. In this review, we present the key aspects involved in the use of these techniques in the catalysis field. Firstly, we introduce some of the fundamentals of the techniques and describe their main features and their impact in the catalyst design. Then, we analyze key examples of the use of SAS to study catalysts' structure through *ex situ* analysis, focusing on examples involving different porous materials and metallic nanoparticles. Afterwards, we discuss *in situ* and *operando* approaches for studying catalytical processes monitored using SAS. Finally, we present perspectives and challenges for the future use of SAS in the catalysis field.

1) Introduction

Catalysts are one of the quintessential components in modern day chemical processes. Nowadays, the majority of the industrial processes used to obtain chemical products are accelerated thanks to the use of catalysts.[1] In the context of environmental concerns regarding pollution and climate change, they will also play a key role in the future for minimizing the impact of social and industrial related activities. In fact, the use of catalysts is already diminishing energy requirements, lessening the generation of toxic gases and wastes and decomposing dangerous toxic by-products.[2]

Among the various types of catalysts, heterogeneous ones stand out due to their easy separation from reaction media and their reusability.[3] These include porous materials such as zeolites, mesoporous oxides and metal organic frameworks (MOFs)[2a, 4] and metallic nanoparticles[2b, 3, 5] either separate or combined in composite materials.[1, 2b, 4e, 6]Understanding how catalysts behave and which are the key features that determine their activity is fundamental both to improve the efficiency of their current design and to further develop new catalytical materials. An adequate characterization of the catalyst before, during and after their participation in chemical reactions is fundamental to achieve such goal. This task involves the acquisition of useful data over length-scales which span various orders of magnitude, form the atomic and molecular level (sub nanometer scale) to macroscopic sizes involved in chemical reactors (several meters). Therefore, multiple techniques should be combined to obtain a complete characterization of catalysts and the catalytical processes at all length-scales involved.[7] For instance, spectroscopic techniques (*e.g.* Infrared, Raman, UV-visible and X-Ray absorption, Nuclear Magnetic Resonance, X-Ray Photoelectron Spectroscopy) are used to understand catalysts at molecular level. On the other extreme of the scale, the activity and efficiency of catalysts are determined using model reactors in which the composition of the fluid phases involved in the catalytic reactions are monitored before, during and after them.

The gap in between these two extremes corresponds to the nanoscale regime, which is particularly important in heterogeneous catalysis. Typically, adsorption/desorption techniques, X-Ray diffraction, electronic microscopies and probe microscopies are used to characterize the size, shape and porosity of catalysts. And it is in this particular length scale that Small Angle Scattering (SAS) measurements stand out as valuable characterization tools.[8] In contrast with electron microscopy imaging, these techniques give information about a comparatively large amount of sample since bulk quantities can be analyzed without compromising their integrity. Moreover, SAS experiments can be performed on a wide variety of aggregation states (solid, liquids, gels) and sample conditions (*e.g.* under different atmospheres or controlled humidity, pressure or temperature), including *in situ* and *operando* measurements. In other words, they are nondestructive and can be used under realistic conditions.[7b, 8]

This review will be dedicated to recent advances in the use of SAS techniques to study catalysts and catalytic reactions, highlighting the interest and potentialities of such methods to obtain key information that will allow the further development of the catalysis field. Firstly, we will present the generalities of SAS techniques, Small Angle X Ray Scattering (SAXS) and Small Angle Neutron Scattering (SANS), describing their main features and the kind of information that can be obtained from them. Then, we will present and analyze recent examples of the use of both SAS techniques to study catalysts structure through *ex situ* analysis, focusing on porous materials

and metallic nanoparticles. Afterwards, we will discuss *in situ* and *operando* studies of catalytic processes performed by SAS. Finally, we will finish the review with some perspectives and challenges for the future use of SAS techniques in the catalysis field.

1.1 Basics of the SAS techniques

SAS consists on extracting information about the characteristics of a sample at the nanoscale by measuring the spatial distribution of the coherent radiation elastically scattered by it at low angles. The lower the angle of scattering probed, the larger the length scales probed by the experiment. Merely as an indicative order of magnitude, we can consider small-angles as 10° and below[9], both for experiments using either cold neutrons or X-rays from an spectral line such as Cu Kα. Thus, in SAS experiments the detector must be positioned at a long distance from the sample in order to obtain an adequate resolution without the interference of the transmitted beam.[8b] In fact, the sample – detector distance can be varied in most SAS equipments; hence, SAS instruments can probe length scales from few Å to about a few hundred nm.[9b] A scheme of the typical steps involved in a general SAS experiment is presented in **Figure 1**.

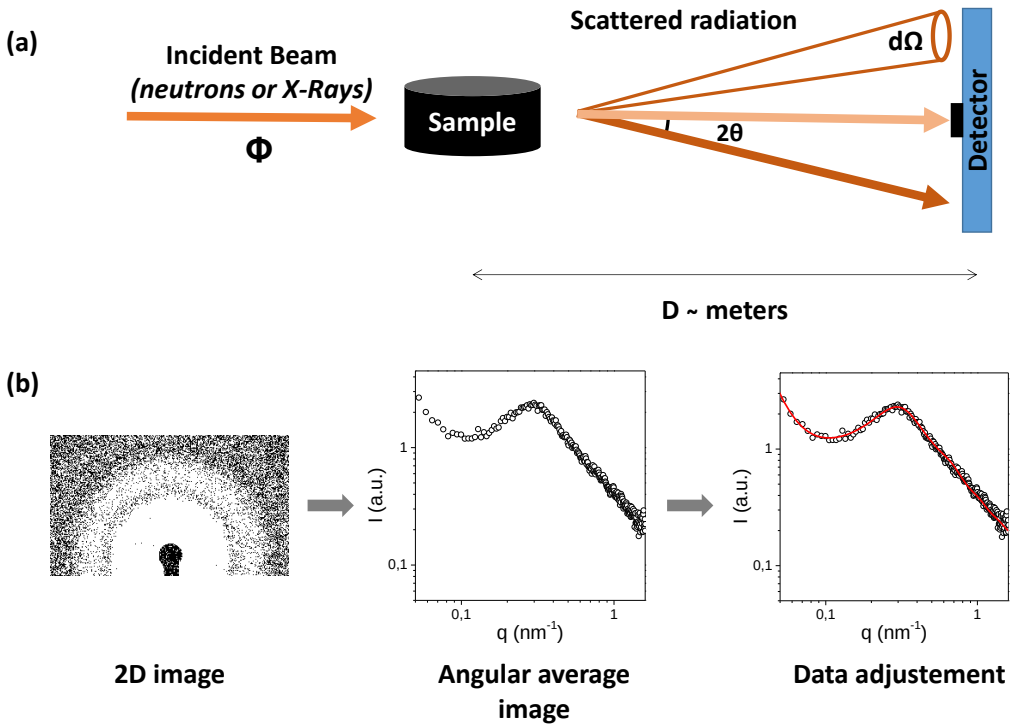

Figure 1. Schematic representation of the steps of a SAS experiment: **(a)** Diagram of the scattering measurement, showing the incident beam, the sample, the scattered beam and the

detector. The flux Φ of incoming radiation is defined as the number of particles per second crossing a unitary area normal to the incoming beam. The cross section is defined as the number of particles scattered in a given direction per unit solid angle divided by the incoming flux Φ. **(b)** SAS data treatment required to obtain useful information from the experiment.

The presence of a small-angle scattering signal is due to changes, within the sample, of electronic density, in the case of X-rays, or of a function called *scattering length density,* in the case of neutrons. The concept of scattering length density can also be extended for X-ray scattering, defining it as the classical radius of the electron times the electronic density. The scattering length density has units of cm^{-2} (with typical values in the order of $10^{10} cm^{-2} = 10^{-6} Å^{-2}$) and reflects the local capacity to scatter particles elastically.

The main objective of a SAS experiment is to determine the *scattering cross section*, since it contains information on the shape, size, and correlations between the scattering centers in the sample.[9b] The *scattering cross section* is defined as the number of particles scattered in a given direction per unit solid angle divided by the incident flux Φ (*i.e.* the number of particles of the incoming beam crossing a transversal unit area per unit time), as seen in Equation 1 and Figure 1a.

$$\frac{d\sigma}{d\Omega} = \frac{(\#particles\ scattered\ into\ d\Omega)/d\Omega}{\Phi} \tag{1}$$

Under the assumption of weak scattering, the cross section can be related to the scattering length density $\rho(\vec{r})$ of the sample through the following relation:

$$\frac{d\sigma}{d\Omega} = \left| \int \rho(\vec{r})\, e^{-i\vec{q}\vec{r}} d^3\vec{r} \right|^2 \tag{2}$$

Here, $\vec{q}$ is a *reciprocal space* vector that represents the momentum transfer from the incident beam to the sample during the scattering event, and $\vec{r}$ represents the ordinary vector position in *real space*. Since we are considering only elastic scattering, $\vec{q}$ modulus is determined by the wavelength λ of the incoming beam by the relation:

$$q = \frac{4\pi}{\lambda} \sin\theta \tag{3}$$

where the angle 2θ is the scattering angle (*i.e.* the angle between incoming and scattered beam). The measured intensity pattern is given by the square modulus of the Fourier transform of the scattering length density, and, consequently, information about the phase is lost. This implies that $\rho(\vec{r})$ cannot be obtained by anti-transforming the measured pattern, and data analysis is not always straightforward, requiring an appropriate model to interpret SAS results.

Figure 2 illustrates the kind of information that SAS can provide, in comparison with ordinary large-angle diffraction measurements. Figure 2a shows the simulated diffraction pattern of 2D square particles (that mimic atoms) arranged in a square lattice, forming a "2D nanoparticle". The diffraction pattern shows a series of Bragg peaks, somewhat widened by the limited size of the crystallite as expected by the Scherrer equation. A signal around q = 0 (i.*e.* at low scattering angles) is also present. While the Bragg peaks correspond to the square crystalline lattice of the ordered atoms, the signal at small angles is due to the shape of the nanoparticle itself. It is worth noting that the structure at smaller length scales (atomic ordering) gives rise to a signal at high q (large angles), while structure at large length scales (size of the nanoparticle) originates signal at low q (low angles). This exemplifies the inverse relationship which exists between length scales in real space and in the q-space (reciprocal space). Interestingly, some experimental setups allow the simultaneous measurement of Bragg peaks and small angle signals, as will be exemplified in section 2.2.

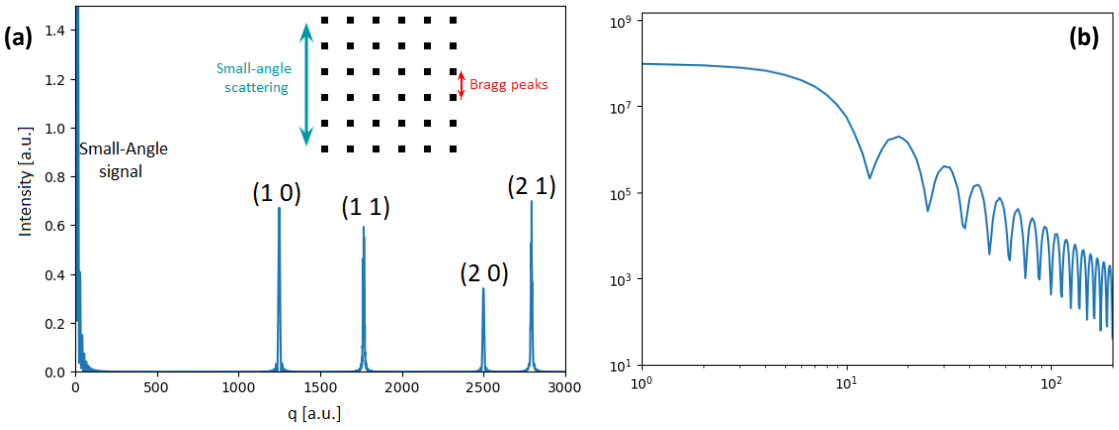

Figure 2. (a) Bragg peaks and small-angle signal originated from different length scales in a square arrangement of 2D particles, shown in the inset. **(b)** Detail of the small-angle signal, in double-logarithmic scale.

When the system under study presents cylindrical symmetry, the data is usually presented as an angular average of the 2D pattern measured in the detector, resulting in a single curve of scattered intensity as a function of *q*, as schematized in Figure 1b. Since the relevant variable is

q, the pattern results are independent of the wavelength chosen for the experiment, making easier the comparison between different measurements. Moreover, it is possible to access different *q*-ranges in a single experiment by varying the wavelength, and later combine both measurements into a single curve.

As an example, Figure 3a presents a typical pattern of the curve expected from an infinitely dilute solution of monodisperse spherical particles, representing the *form factor* of the spheres. The sharp minima are related to the radius of the particles; larger particles result in smaller values of *q* at each minima. In practice, these are smoothed by effects of polydispersity and finite collimation. If the sample consists of non-spherical particles, the SAS signal will correspond to other structure factors, many of which are well known. Some selected examples of model SAXS patterns are shown in Figure 3b. If the solution is not sufficiently diluted, or if aggregation starts to occur, additional structure begins to appear in the curve. This additional structure contains information of the particle distribution, and is therefore called the *structure factor*. Both structure and form factors can be calculated for model systems and fitted to the data (see Figure 1b) to extract useful information about the sample. This interplay between form factor, structure factor, polydispersity limited resolution and instrumental effects contributing to the final scattering means that the data analysis for this technique usually requires additional knowledge about the sample, which must be obtained by complementary techniques.

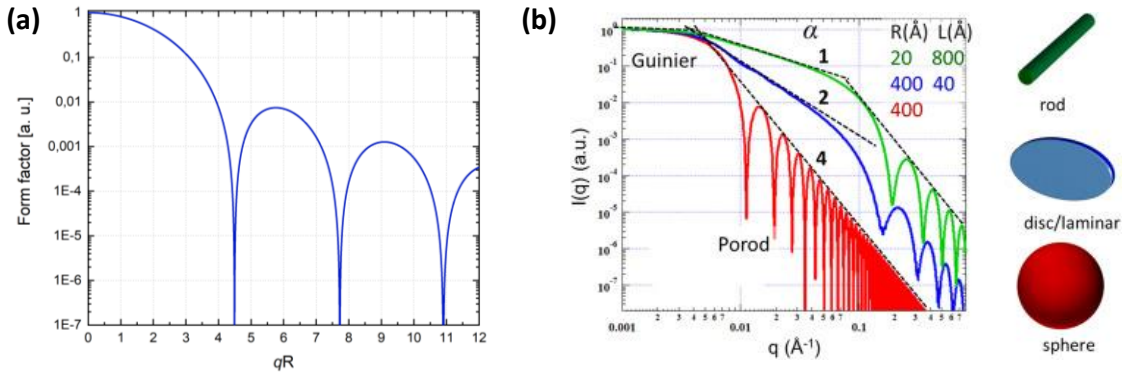

Figure 3 (a) Structure factor of a sphere of radius R. Notice the logarithmic scale and the zeros of the structure factor at precise values of *q*R. **(b)** SAXS patterns of a sphere with a radius (R) of 400 Å, with labeled Guiner and Porod regions (red curve), a disc with R= 400 Å and thickness L= 40 Å (blue curve) and a long rod with R= 20 Å and length L= 800 Å (green). Reprinted from reference [10], Copyright (2018), with permission from Elsevier.

Nonetheless, there is also model-independent information that can be extracted from SAS experiments. For example, for a set of diluted scatterers of constant scattering length density,

the radius of gyration R_g (a geometrical property related to the mass distribution and size) can be obtained from the low q asymptotic using the so-called Guinier law. Similarly, the behavior at higher q is dominated by a power law exponent related to the surface of the scatterers (Porod law), or to the fractal dimension in the case of fractal systems.[11]

In addition to the more standard measurements of SAS described above, there are several variations of the typical configuration setup. For instance, Grazing-Incidence Small-Angle Scattering (GISAS) is useful for probing nanostructures of thin films and other nanostructured surfaces and is based on the beam incidence over a flat sample occurring at precisely controlled small angles (see later in section 2.1.3). It usually works on reflection mode and an area detector is imperative; a good review on GISANS can be found at reference. [12] Another alternative is Ultra-Small Angle Scattering, a technique that can be used to probe larger structures. The instrumental setup for this kind of measurements usually follows a Bonse-Hart configuration, very different from the one described above. Finally, Anomalous Small-Angle X-ray Scattering (ASAXS) can also be used, where SAXS patterns are measured at different wavelengths, close to X-ray absorption edges of an element present in the sample. Under these conditions, an anomalous behavior of the contrast for such element allows to distinguish element-specific contributions to X-ray scattering.

1.2 SAXS

As explained before, the interaction of X-Rays with matter occurs primarily with the electronic clouds of the atoms. Thanks to such interaction, SAXS experiments can give information on particle sizes and shape, size distributions, surface area and, in some cases, surface roughness. Moreover, in the case of ordered porous materials, information of such ordering can be extracted. In this point, it is important to consider that the scattering length grows monotonically with the atomic number Z and, therefore, light atoms or atoms with similar Z may not provide enough contrast to perform a measurement in a reasonable time.

SAXS measurements can be carried on either using commercial equipment or using specially-designed synchrotron sources.[7a, 7b, 13] In both cases, the detection of radiation is generally performed with a 2D array of pixels such as Hybrid Photon Counting detectors. The range of accessible q will depend on the detector size and the available possible distances between the sample and the detector.

Commercial SAXS devices typically use Cu or Mo anodes for providing the X-Ray flux, whose output (i.e. the intensity of the beam) is mainly limited by the cooling mechanism. Rotating anode sources are an alternative for higher flux on laboratory sources. Synchrotron sources, on

the other hand, are large facilities which provide much higher fluxes, with polarized, highly collimated beams of tunable wavelength. A higher flux means that each data acquisition takes less time and with higher temporal resolution. As a rule of thumb, laboratory equipment is better for *ex situ* characterization of catalysts, while synchrotron sources are preferred for *in situ* and *operando* experiments. However, in the latter case, care should be taken with the radiation damage due to large flux, which may influence the obtained results.

1.3 SANS

The information that can be obtained by SANS is, in general terms, equivalent to the one that can be extracted by SAXS measurements. However, neutrons present a set of advantages with respect to X-Rays, making them especially suited for problems which are difficult to tackle with X-Rays. Essentially, these advantages are due to the interaction mechanism between the sample and the neutron beam, that involves the nuclei and not the electronic clouds, as it is the case for X-Rays. The scattering length density varies both non-monotonically with atomic number and for different isotopes of the same element.[14] This allows to have good contrast between elements with similar atomic numbers, which are not always distinguishable by X-Rays and to perform contrast variation by deuteration or isotopic substitution. Moreover, the interaction of the neutron beam with the sample is usually weaker than that with X-Rays resulting in a higher penetration capacity, that potentially allow *in situ* characterization of catalysts under extreme conditions.[7b] Such weaker interaction also implies lower sample damage due to radiation. However, there is a negative consequence as the requirement of longer measurement times hampers the temporal resolution.

Neutrons are usually obtained as a product of fission fuel in the core of a nuclear reactor or as the consequence of the bombardment of heavy nuclei by energetic ions in spallation sources.[13] These sources are relatively scarce around the world, and their usage is subject to a system of proposal evaluation which often results in oversubscribed instruments. In addition, the neutron flux at currently available sources is low and large volume samples and long exposures are required to obtain information with an adequate signal-to-noise ratio. These aspects impact on the experiment duration, limiting the acquisition of kinetic information.[7b] Consequently, the use of SANS is far less usual than SAXS in the catalysis community.

2) Discussion of recent literature

2.1 *Ex situ* experiments

In the last decades, nanosized and nanostructured materials gained relevance in the catalysis field due to their large surface to volume ratio as well as the possibility to offer reactive sites based on different crystal planes with controlled structural defects and with complex chemical composition. At the same time, nanomaterials comprise different chemical compositions such as metal oxides, non-metal oxides, pure metals, alloys, etc., together with different geometries and particles and pore sizes. Among this diversity, we highlight here the study of porous oxides and metals, MOFs and metallic nanoparticles (NPs) in the last 10 years. These particular materials present confinement effects which enhance their catalytic performance and stability.[15] Within this group, mesoporous materials are attractive because they offer a solid support, protection and selectivity to the catalytic sites.[16] On the other hand, MOFs research on catalysis is gaining momentum given their versatile multiple chemical composition and combination with functional groups.[17] Finally, the study of NPs is extended and comprises metallic ones with different shapes and sizes, and used as part of several matrixes (in suspension, included in core-shell structures, supported in mesoporous frameworks, supported onto plane substrates).[3, 18]

In the cases mentioned above, in addition to their chemical composition, the dimensions and geometry of the catalysts are critical to their performance. For this purpose, a vast analysis using complementary techniques is strongly recommended.[19] However, as explained before, the characterization by means of SAS techniques provides information about size, shape and spatial distribution of nanosized objects averaging a larger portion of sample compared to electron and atomic force microscopies techniques. During the data analysis of these systems, a model has to be applied requiring information obtained by other experiments, and particular care needs to be taken when interpreting scattering signal intensity.[20] Most of the SAXS and SANS analysis found aim to evaluate the long-range order of mesoporous structures before the catalytic reaction takes place while their performance is analysed in terms of their turnover rate or other kinetic parameters. However, as we will see, Gommes *et al.* pointed out that the scattering pattern contains much more structural information other than simple periodicity of the structure.[8b] In this context, both SAXS and SANS do not interrogate directly the surface chemistry and give a general picture of the surface´s structure or long-range order degree. Despite this apparent weakness, *ex situ* analysis of catalysts is the simplest form for comparing the various chemical and physical changes before and after the catalytic action. Strangely enough, few reports give an account of the catalyst and/or mesoporous framework fate after operational conditions.[21]

2.1.1 Mesoporous frameworks: inorganic oxide-based materials and other templates

Mesoporous frameworks possess higher specific surface areas and larger porosities when compared to general bulk materials. This is an obvious and useful trait for catalysis when active NPs are anchored to the pores walls or active atom sites are embedded along the mesoporous structure. Typically, mesoporous systems are structures with a long-range order dictated by the cooperative self-assembly of molecular building blocks during synthesis.[22] Given that this order is in the range from 2 – 30 nm, SAXS and SANS are the natural tools for probing these dimensions. It must be noted too, that there is a considerable body of work on using these techniques for studying the self-assembly and assisted chemical synthetic processes that lead to these organized porous materials. [23] However, in the following paragraphs we will address what is considered the "final object", that is the NPs/active sites embedded in the mesoporous framework.

Among the catalytic mesoporous supports more frequently found, mesoporous SiO_2 matrices excel as solid supports for integrating catalytic particles or chemical groups (*i.e.* MCM-41, SBA-15 and SBA-16). Their simple synthetic setups, reproducibility, easy surface functionalization and characterization provide an amenable catalytic platform. For example, SAXS analysis of SBA-15 based materials is based on equation 4 which corresponds to a general hexagonal symmetry, with the *l* parameter equal to zero (all peaks correspond to (*hk0*) planes), *a*, the cell parameter and *d* is the interplanar spacing and represents the pore-to-pore distance [100] plane, too.

$$\frac{1}{d^2} = \frac{4}{3}\left(\frac{h^2 + hk + k^2}{a^2}\right) + \frac{l^2}{c^2} \qquad (4)$$

The indexing of the peaks corresponds to the [100], [110] and [200] planes and is representative of a 2D hexagonal structure (space group *p6mm*). For instance, Beejapur *et al.* compared the performance of sulfonic groups immobilized onto SiO_2-particles and mesoporous SBA-15 as acidic catalysts for the glycerol acetylation.[24] They confirmed from SAXS measurements that the typical SBA-15 porous structure is maintained after the incorporation of the sulfonic groups, as the peaks do not show any shift and have a very weak intensity loss, attributed to pores filling with the sulfonic groups (shown in Figure 4a). The same mesoporous SiO_2 framework can be applied as a shell on various nanoparticles enabling their protection from the surrounding environment and controlling the solvent and reactants accessibility. Xiao *et al.* synthesized Pt NPs within aligned mesoporous silica wells in SiO_2 core-shell particles (see Figure 4b).[25] In this

case, SAXS gave information about the CTAB-templated porous structure present in the SiO_2 shell surrounding the NPs, as shown in Figure 4c. The authors attributed the 1:2 ratio observed for the peak positions to a lamellar disposition of a small domain of four pore channels (center to center distance ~3.6 nm). As previous reports noted, either broad or the absence of higher order reflections suggest that ordered mesopores do not form large diffraction domains on thin and curved shells due to geometrical constraints.[26] Also, the authors evaluated the catalytic activity of these composites for ethylene hydrogenation and the accessibility of the reactant to the Pt NPs by pore diffusion. Catalyst deactivation due to carbon deposition after dehydrogenation was solved by means of a high-temperature combustion treatment of the Pt/SiO_2 NPs. Again, catalyst reuse was only evaluated from kinetic experiments.[25]

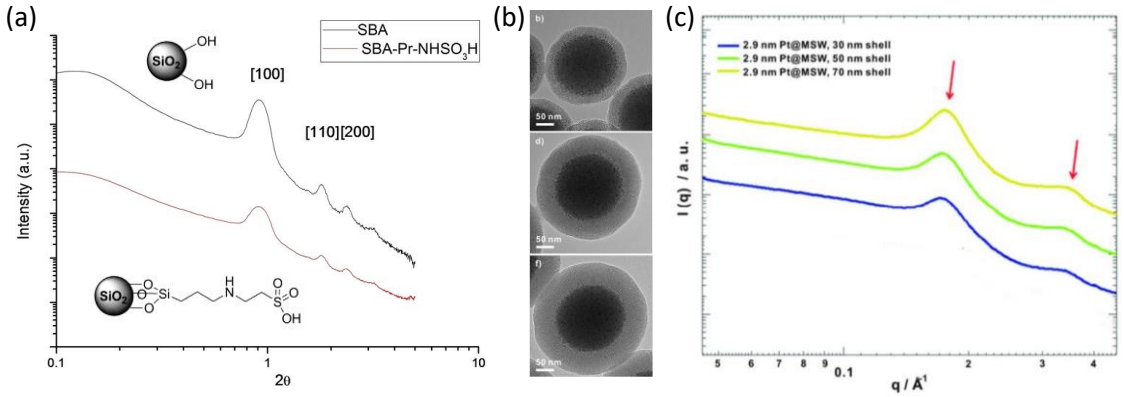

Figure 4. **(a)** SAXS patterns and schemes of SBA-15 and sulfonic SBA-15 catalysts. Adapted with permission from reference [24]. **(b)** Transmission Electron Microscopy (TEM) image of Pt NPs (small dark spots) loaded onto NH_2-functionalized SiO_2 spheres with 30 (top), 50 (middle), and 70 nm (bottom) layer mesoporous SiO_2 shells and **(c)** SAXS patterns of the samples shown in (b). Adapted, with permission, from reference [25].

In the following examples we will present this typical approach for SAXS measurements for catalytic NPs, chemical groups or active site dispersed on various mesoporous supports.

The first example worth discussing is the one presented by Böttcher *et al.*: the authors studied the enantioselective hydrogenation of ethyl pyruvate using Pt-supported ordered mesoporous SiO_2 materials (SBA-15, SBA-16 and KIT-6) along with cinchonidine.[20d] They confirmed that the framework pore wide-range ordering was not affected after the incorporation of Pt within SBA-15, and that some degree of shrinkage of the structure happened for the other systems from SAXS powder diffractograms. The enantioselective hydrogenation of ethyl pyruvate was

attributed to slight changes of Pt nanoparticle morphology according to SiO_2 mesopore environment, dependent on Pt (111)/Pt (100) ratios.

Biocatalytical frameworks have also been evaluated. Gustafsson *et al.* employed SAXS for checking the encapsulation of trypsin and lipase within SBA-15 SiO_2 particles. Different pore sizes (5 nm, 6 nm and 8.9 nm) and morphological information of the starting material were studied. [27] Another modification of mesoporous silica was made by Maheswari *et al*. who incorporated variable amounts of W into SBA-16 SiO_2 (cubic *Im3m*) structure *via* a one-pot synthesis and carried on a cyclohexene oxidation.[28] Under variable W loading, the mesoporous framework kept the long-range order until reaching a ratio of Si/W = 10; at this loading, both a sharp decrease in surface area and pore volume of the platform were observed. Although the authors suggested a disruption of the *Im3m* structure long range order, these results can be explained in terms of the changes in the periodic electron density of the nanocomposites before and after W infiltration.

Another interesting example is the one discussed by Castanheira *et al.,* who obtained photocatalytic TiO_2 NPs hydrolysing titanium (IV) isopropoxide within the mesoporous channels of SBA-15. The typical reflections of 2D-hexagonal mesostructures of the porous silica matrix were observed under SAXS even with variable TiO_2 NPs loadings (from 10 % to 30 % w/w), confirming that the SBA-15 matrix resisted the post-synthesis modification. Once again, the catalyst reuse was only evaluated from kinetic experiments. [29] Other inorganic species can be encapsulated within porous SiO_2; for instance Bhunia *et al*. anchored vanadium (IV) using orthohydroxy-acetophenone onto amino-modified MCM-41 for bromination of hydroxy aromatic compounds.[20a] They observed from SAXS measurements that after post-synthesis grafting, the intensity of the diffraction lines decreased. Multiple motives were invoked: lowering of the mesoporous local order, variations in the wall thickness, as well as the reduction of scattering contrast between the channel wall of the silicate framework and the vanadium complex. Similarly, more complex oxides can be included within the porous framework, as shown by Janssens *et al*., who synthesized ternary Ag/MgO catalysts in SiO_2 mesoporous powders for the conversion of ethanol into butadiene. SAXS measurements were used to check if the mesoporous ordering of the MCM-41 and COK-12 frameworks endured the dry milling for obtaining the MgO.[30] Similar examples of before/after precursors imbibement within mesoporous matrices can be found in the literature.[31]

As we mentioned before, SAXS pattern reveals structural information that lies beyond the long-range correlation of the structure.[8b, 32] In this context, Gommes *et al.* provided the theoretical framework for the general analysis of X-Ray scattering data of NPs-loaded pores in micro, meso, and macroporous materials using SBA-15 as a model.[16b, 33] Analysing the SAXS from the loading

of the SiO_2 powders with Cu NPs under different heat treatments/mixture gases (N_2, NO/N_2) they assumed two different situations: a) a random loading for the mesopores and empty micropores and b) the formation of "patches" of loaded pores. This allowed them to distinguish different conditions such as Cu NPs only present in the mesopores or the presence of the Cu precursor (e.g., $Cu(NO_3)_2$) both in the meso- and micropores.

Other SAXS-derived techniques enable the identification of atoms along the mesoscopic structure. Radnik *et al*. studied Cu containing silicoaluminophosphates (SAPO) using ASAXS, a technique useful for separating the scattering contribution of a certain element from others in the sample, based on the resonant behaviour near its absorption edge. [34] Combination of ASAXS with X-Ray Absorption Fine Spectroscopy (XAFS) showed that excessive impregnation of Cu precursors led to the formation of a CuO shell. Cu-SAPO catalysts are potential catalysts for reduction/oxidation reactions (e.g. NOx reduction or oxidative carboxylation).

In essence, SAXS characterization of porous systems is likewise carried on for other oxides and metal-based materials including TiO_2,[35] aluminosilicate,[36] C_3N_4,[37] Cr_2O_3,[20c] Fe_2O_3, [38] and carbon-Nb_2O_5.[39] Electrodeposited metals from lyotropic liquid crystals soft templates Pd,[40] and Pt and Pt/Ru alloy [41] for fuel cell applications are also easily characterized.

Besides the analysis of chemical building block precursors, in which SANS has excelled as a technique for characterizing the firsts steps on the formation of mesoporous structures, SANS has found a niche when probing the obtained mesoporous structures used as catalytical platforms.

Forgács *et al*. studied the immobilization of 1,4,7,10-tetraazacyclododecane [Cu(II)-cyclen] molecules in a mesoporous silica aerogel as a catalyst for the oxidation of phenol by H_2O_2.[42] SANS curves of CuCy-AG samples showed no specific scattering due to the contrast of nanosized objects when using H_2O – D_2O mixture that matched the neutron scattering length density (SLD) of amorphous silica. This indicates that the anchored Cu(II)-cyclen groups are dispersed homogeneously within the functionalized silica aerogel and do not aggregate, a result later supported by EPR experiments. If formation of Cu(II) containing clusters were expected, scattering from these sites would be observed when the contrast of silica is matched.

Likewise, Rahman *et al*. relied on contrast matching SANS measurements using H_2O and D_2O mixtures for testing the pore accessibility of Co-catalysts embedded in hexagonally ordered mesoporous SiO_2.[43] This catalyst was evaluated for styrene epoxidation reaction and SANS demonstrated that the cobalt moieties were evenly dispersed as they kept the pores accessible to the reactants and products. Kumar *et al*. performed a similar experiment using the CO_2 adsorption as a contrast agent on an In oxide supported SBA-15 for the vapour phase Beckmann rearrangement of cyclohexanone oxime.[44]

Finally, Chabot *et al*. employed SANS for studying the ionomer and water distributions at different relative humidity and contrasts in proton exchange membrane fuel cells as the Pt content in the electrode. In these systems the electrode platinum content and its relation with the catalyst layer structure and the water and ionomer distributions define the availability of the active sites for electrochemical reaction. [45]

2.1.2 MOFs

In the last decade, the use of MOFs in catalysis gained relevance as promising materials with highly controlled pore dimensions and chemistry. As MOFs are composed of repeating building blocks constructed from positively charged metal ions/complexes and bridged by organic molecules, SAXS helps to identify the presence of mesopores within the crystallized framework or, in the initial formation stage of the reticular network, the assembly of molecular clusters in solution.[46] For instance, Wang *et al.* demonstrated the formation of a supramolecular metal-organic framework (SMOF-1) in water at room temperature composed of $[Ru(bpy)_3]^{2+}$ and cucurbit[8]uril, performing SAXS on the liquid solution, which coincided with a cubic structure with a *d*-space centred at around 3.1 nm (see Figure 5a).[46a] In turn, higher Miller indices of the supramolecular clusters were obtained using solution-phase synchrotron X-ray diffraction, characterized with broad signals as seen in Figure 5b. The catalytical activity of this SMOF-1 structure relies on the adsorption of anionic Wells-Dawson-type polyoxometalates that carry a photo-driven H_2 production. Similarly, Zhang *et al*. synthesized an intertwined $[Ru(tpy)_2]^{2+}$ (tpy = 2,2',6',2''-terpyridine) complex and cucurbit[8]uril for alcohol oxidation and employed a combination of SAXS and solid X-ray diffraction to infer a simulated woven supramolecular MOF.[46b] As we have seen for silica based materials (e.g. SBA), Mor *et al*. used SAXS for the analysis of mesopores size distribution in hollow frameworks based on ZIF-67/ZIF-8 (core/shell) MOFs as a function of ZIF-67 dissolution.[46c]

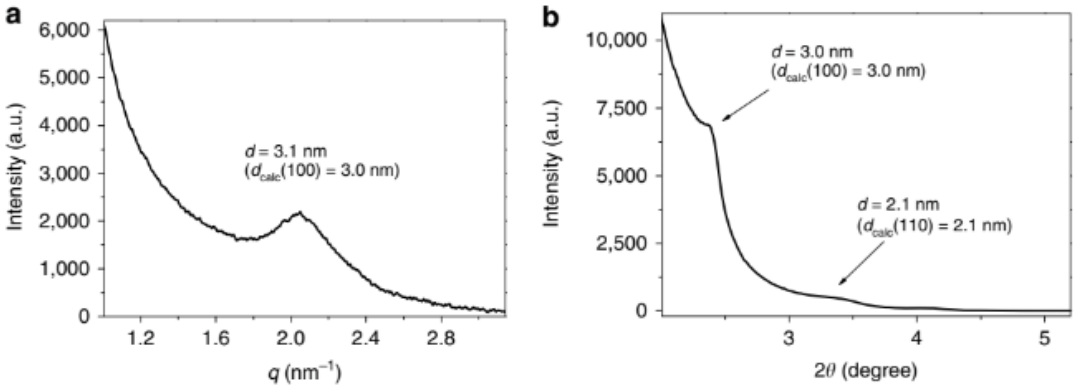

Figure 5 (a) Synchrotron SAXS of a 3 mM supramolecular metal-organic framework (SMOF-1) composed of $[Ru(bpy)_3]^{2+}$ and cucurbit[8]uril aqueous solution; (b) synchrotron X-ray diffraction of the same solution; note that this technique achieves smaller correlation length distances compared to SAXS. Used under Creative Commons CC BY license from reference [46a].

2.1.3 Bare nanoparticles

Non-porous nanoparticles (metallic, oxides, etc.) are highly attractive for catalysis applications either if they are dispersed in a liquid medium or supported on solid substrates. In all these cases, SAXS is used to characterize NPs size and, if present, their spatial correlation.[47] For example, Heilmann *et al*. described the synthesis NiCu core-shell nanoparticles (see Figure 6a) for the reverse water-gas shift reaction.[48] From SAXS patterns analysis, shown in Figure 6b, they concluded that NPs diameter was 6.8 nm with a distribution of 14% using a Weibull distribution. While SAXS allowed the integral modelling of the core-shell structure, ASAXS enabled to perform element specific structural analysis. In particular, the effective electron density of Ni, Cu, and NiO was interpreted according to a core-shell structure. Wang *et al*. analysed with SAXS the mesoscale structure of AuPt hollow nanospheres (Figure 6c) and the sequential changes along the synthetic steps.[49] The SAXS patterns they obtained from AuPt nanospheres and Au nanospheres showed a ring type diffraction (Figure 6d) attributed to hollow particles. The methanol electrochemical oxidation reaction was evaluated for their potential applications as catalysts.

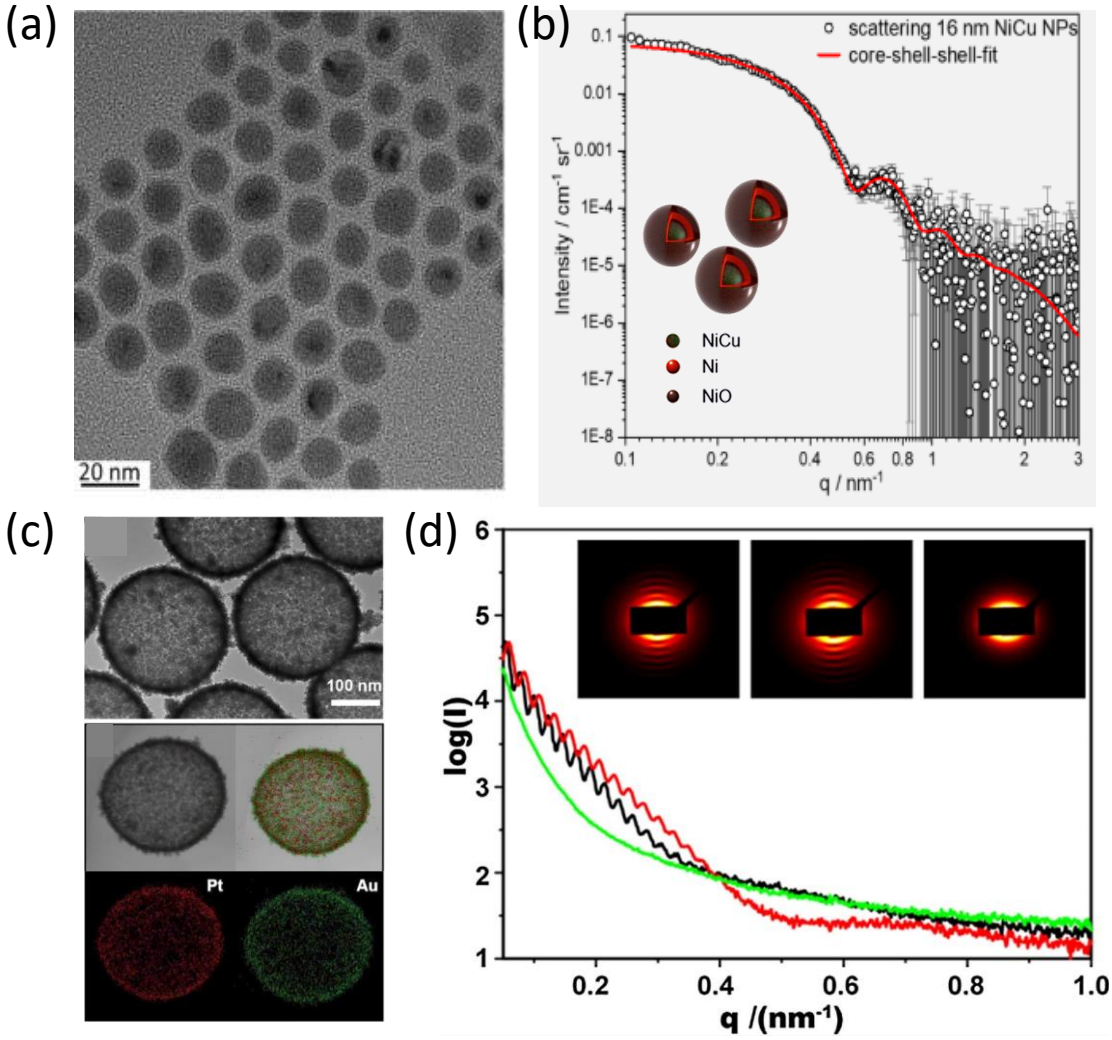

Figure 6. (a) TEM images of spherical 16 nm diameter NiCu nanoparticles and **(b)** SAXS curve of the same particles (black circles) and the fitted curve using a core–shell–shell model (red line). Adapted, with permission, from reference [48]. **(c)** TEM image of hollow porous AuPt nanostructures (top), scanning TEM images and elemental mapping images of distribution of Pt (red) and Au (green) in those nanostructures (middle and bottom) and **(d)** SAXS curves of hollow Au nanoshells (red line), hollow porous AuPt nanoshells (black line) and Pt nanoparticles (green line), respectively; and their respective SAXS patterns (insets from left to right). Adapted, with permission, from reference [49].

Kronawitt *et al*. employed SAXS for analyzing poly(p-xylylene)/polylactide/Au NPs composite non-woven mesotubes with non-agglomerated NPs used for the hydrogenation of dimethylphenylsilane. SAXS measurement confirmed that there was no change of the NPs size after extraction of the PLA sacrificial template.[50]

Burato *et al.* analysed the influence of the PVP capping agent used for protecting Pd NPs on the hydrogenation of unsaturated carbon-carbon bonds. Given that the X-Ray scattering parameters

agreed with Transmission Electron Microscopy (TEM) observations, they concluded that the NPs mean size were not affected by the purification procedure, and could be ruled out when comparing their catalytic activities.[51] Similar structure analysis can be found for ZnO, [52] ZrO_2,[53] WO_3,[54] Pd, [55] Pt, [21b, 56] and Au[57] nanoparticles.

Several researchers turned to SANS in order to measure the distribution of metal NPs adsorbed on carbon-based matrices, generally employed in fuel cell devices or electrochemical setups. The NPs are usually transferred to the platform using a catalytic ink, consisting of the metallic NPs (*e.g*. Pt, Pt/Ru, Co, etc.) mixed with ionomer solutions, a carbon powder (Vulcan powder, carbon nanotubes, etc.) and a dispersing solvent. In this context, several researchers aim to reveal the amount of non-adsorbed ionomer in the catalyst ink or the NPs distribution along the nano-sized support using contrast-variation SANS (CV-SANS). [58] Also distribution of fillers (*e.g*. SiO_2) and ZnO NPs in rubber as catalyst for the vulcanization process has been analyzed using CV-SANS, considering the unfilled rubber as a three-component mixture made of processing oil, rubber, and ZnO NPs which lead to different scattering contrasts. This allows to discriminate the contribution of silica and ZnO in the final composite.[59]

In an impressive demonstration of the combined power of SANS and ultra-small angle neutron scattering (USANS) for material characterization, Kim *et al*. studied the morphological features of two different commercial γ-Al_2O_3 used as a Pt- support and as matrix in automobile exhaust catalysts. Both techniques combined spanned almost four orders of length scales, from the nanometer to the micrometer scale, providing a complete description of both systems. Moreover, this enabled to distinguish that, in one case, the material was composed from aggregates of 2-3 stacks of platelet-like particles and, on the other, from random aggregates of rod-like particles. The authors analyzed the Van der Waals interactions between the two particle shapes and the aggregate geometry, concluding that the platelet-like NPs had stronger interactions leading to compact structures that left limited available surface area (*i.e*. terraces and kinks) while the rod-like NPs were loosely aggregated with a better surface/volume ratio. Further TEM analysis showed a homogeneous distribution of the Pt NPs along these rod-like supports that further correlated with a better efficiency as a three-way catalyst component for the oxidation of hydrocarbons, CO and NO.[60]

CV-SANS can be also used for analyzing and characterizing the presence of fouling adsorbates from a deactivated Ru/C catalyst used for supercritical water gasification as carbon scatters strongly thermal neutrons.[61] In the same work, the authors tackled the identification of carbonaceous materials on spent catalysts too, using ultrahigh-pressure liquid chromatography coupled with hyphenated high-resolution mass spectrometry (UHPLC-HRMS). Obviously, the latter method proves to be less complicated in terms of instrument requirements but, it is

interesting to propose the detection of a very thin layer of C-based materials on NPs surfaces with no sample processing whatsoever.

Catalytical NPs or mesoporous materials can be immobilized on plane substrates too.[3] When these sort of materials are studied, grazing incidence SAXS (GISAXS) must be used (depicted in Figure 7a) as it helps on the determination of the NPs size, surface coverage and their distribution. For example, Dendooven *et al.* used GISAXS *in* and *ex situ* to monitor the growth of well-defined Pt NPs using atomic layer deposition of a Pt precursor, trimethyl(methylcyclopentadienyl)platinum, oxygen and a N_2^+ plasma.[62] Modifying the synthesis conditions they obtained NPs with diameter between 5 to 11 nm and found a substrate coverage ranging from 35 to 280 atoms per nm^2, impacting on the electrocatalytic performance of the substrate for the hydrogen evolution reaction. In other works, GISAXS determined the long-range pore arrangement of mesoporous TiO_2 thin films deposited onto ITO substrates for photocatalytical decomposition of methylene blue.[63] Similarly, Violi *et al.* characterized ZrO_2-CeO_2 mesoporous thin films loaded with Au NPs to catalyze the reduction of nitro-groups by $NaBH_4$.[64] Both normal incidence and grazing incidence configurations were used (Figure 7c) obtaining two different patterns corresponding to the spatial distribution of pores. While SAXS performed on the film at 90° shows a disordered structure in the *z*-direction, the low incidence angle shows a diffraction pattern compatible with a distorted *Im3m* mesopore arrangement in the *xy* plane. GISAXS technique was also extended to viral-templated palladium nanocatalysts onto gold-coated silicon wafers and their stability evaluated under the catalytic reaction conditions (Figure 7b).[21a]

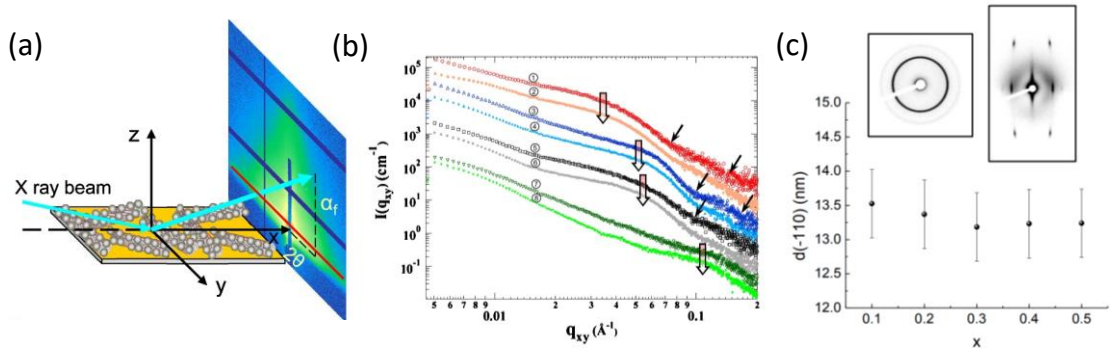

Figure 7. **(a)** Scheme of a GISAXS setup and **(b)** GISAXS curves of Pd nanoparticles of 4 different sizes supported on gold substrates before and after the catalytic reaction. Adapted with permission from reference [21a]. **(c)** Interplanar distance d(-110) of plane of pores as a function of composition (x) of $Zr_xCe_xO_2$ mesoporous thin films and SAXS patterns of a $Zr_{0.7}Ce_{0.3}O_2$ mesoporous thin film obtained at 90° (inset left) and at 3° showing the typical dots pattern for *Im3m* structure (inset right). Adapted with permission from reference [64].

In essence, both SAXS and SANS performed *ex situ* provide valuable information about NPs catalyst size and coverage, pore arrangement of the catalytic platforms and distribution of the catalysts within solid supports. Evidently this approach is much simpler that the design of a specific cell for measuring *operando* conditions. Nonetheless, we detected that in many cases the catalyst characterization is made only before the catalytic reaction.

2.2) *In situ* and *operando* experiments

In this section, we will discuss the use of SAS techniques for *in situ* and *operando* measurements of catalytic process, along with the equipment available for such purposes. Examples will be explored that illustrate the use and application of different sample environments to elucidate catalytic reactions.

To begin discussing the available techniques for *in situ* and *operando* measurements at synchrotron X-Ray and neutron sources, it is important to define these terms. *In situ* experiments involve characterizing a catalyst under working conditions, while *ex situ* characterization, described in the previous section, is performed on the catalyst before or after the reaction. On the other hand, *operando* experiments measure the catalytic activity and selectivity *in situ*, usually by analyzing the outlet of the reactor by Gas Chromatography (GC) or

Mass Spectrometry (MS). This type of experiment is performed in real-time while the catalyst is actively working.

As stated before, one of the major advantages of SAS in catalysis research is its ability to investigate materials under realistic reaction conditions. With the use of a specialized sample environment, researchers can mimic the actual reaction conditions and obtain *in situ* measurements of the catalytic process. This allows for a far more accurate understanding of the reaction mechanisms and how it is affected by different experimental variables, such as temperature, pressure, and catalyst composition.

In addition to providing real-time information about the catalytic process, SAS also allows to investigate the structure of the catalyst and its interaction with the reactants. By analyzing the scattering patterns produced by neutrons or X-Rays interacting with the sample, the size, shape, and distribution of particles in the material can be determined. The information obtained from these experiments can be used to optimize the design of the catalyst to improve its performance. Overall, SAS techniques in catalysis with sample environment represent a significant advancement in catalysis research.

In situ and operating SAS experiments are a valuable tool for studying catalysts under real working conditions. Some common sampling environments used to study catalysts are: temperature, pressurized gas, continuous flow and still flow systems.[65]

These are just some examples of sample environments used in *in situ* and *operando* SAS experiments for the study of catalysts. The choice of sample environment depends on the properties of the catalyst and the experimental conditions required for the specific study.

It is important to note that sample environment equipment and facilities are not just accessories to the experiment, but rather an essential and integral part of it. Common conditioning methods include cryogenic, high-temperature, high-pressure, magnetic fields, viscous flow, gas flow, chemical preparation, or a combination of these techniques. In addition, there may be a need to physically manipulate, reorient, or reposition the sample, while maintaining a high degree of accuracy during the course of the experiment.

To obtain the necessary information to determine the reaction mechanism and imitate the actual operational environment of the heterogeneous catalyst, it is often necessary to combine multiple probes with neutron scattering or X-Ray scattering studies.

Below, we present some relevant examples of the use of SAS techniques for the characterization of catalytic processes.

2.2.1 GISANS with humidity chamber

Ueda *et al.* made a study on the three-phase contact in a fuel cell catalyst layer and water distribution by using GISANS and neutron reflectivity (NR).[66] They utilized two facilities, KWS-1 and iMATERIA, which use monochromatic beam at FRM-II Germany and time-of-flight beam at J-PARC Japan. They fabricated a model catalyst on Si substrates by stacking thin layers of Pt by sputtering and dissolved Nafion and made a solution and deposited by spin coating over Pt film. The sample environment used for the measurements is shown in Figure 8a.

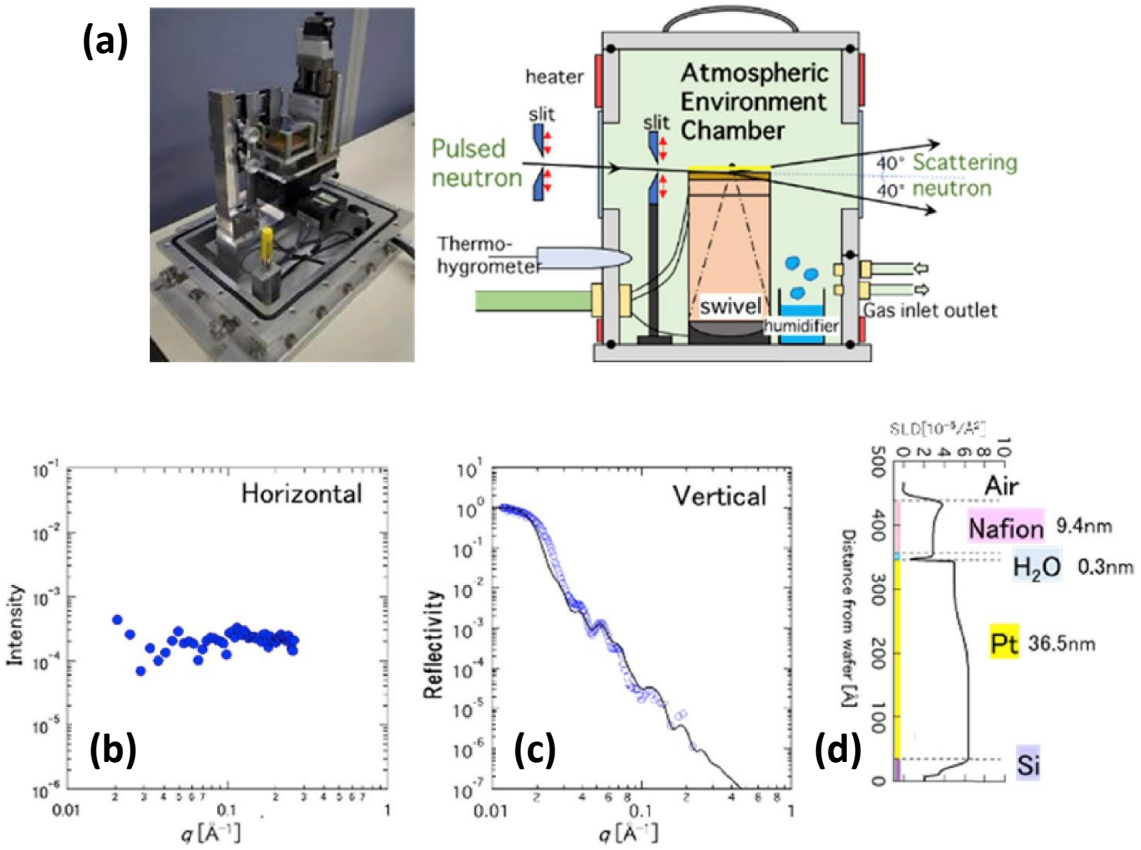

Figure 8 (a) Atmospheric environment chamber using for a power diffractometer iMATERIA (BL20) at MLF, J-PARC, Tokai. **(b)** GISANS and **(c)** NR patterns obtained for humidify the sample of Pt and Nafion with humidification. After analysis, SLD is depicted in real space **(d)**. Reprinted from reference [66], Copyright (2018), with permission from Elsevier.

Figure 8b-d shows the results of the GISANS and NR experiments obtained from the sample with the Nafion layer, which was fully humidified at a controlled temperature. From GISANS (Figure 8b), the authors observed that there is no maximum of ion cluster scattering in the q region around q = 0.15 Å^{-1} in the horizontal direction of the substrate. This observation reveals the absence of ion cluster domains formed on the ionomer thin film prepared on the flat Pt surface. On the other hand, Figure 8c shows the result obtained by NR, observing the sample in the film thickness direction. After analyzing the curves with a MOTOFIT program, a spatial variation of

the SLD along the thickness direction is drawn (Figure 8d). By such analysis, the authors found that a water layer corresponding to the thickness of a molecule (~ 0.3 nm) appears on the Pt surface and that the thickness of the Nafion thin film was 9.4 nm with 7 wt % of water. Moreover, they observed the humidification influence in the vertical direction in Pt flat surface by GISANS. Those experiments confirmed the presence of a water layer between the Pt layer and the Nafion layer and noted an increase in the thickness of the Nafion layer and an increase in the water content of the Nafion thin layer. However, in the horizontal direction, water channels (microphase separation of Nafion) were not observed in the core of the thin Nafion layer.

2.2.2 Reaction Cell with SAXS-XAFS

The following is an example of a reaction cell, where Tan *et al* combined two X-Ray based techniques, XAFS and SAXS, to study catalysts under working conditions.[67] In particular, the researchers conducted several experiments and analyses to investigate the formation process of non-crystalline Ni-P nanoparticles under liquid pulse-discharges.

Figure 9a, shows the reaction cell for the *in situ* XAFS and SAXS measurements. The cell was made of stainless steel with an X-Ray passage of approximately 1 mm and Kapton films were used as X-Ray windows. The cell was placed in an aluminum holder to control its temperature.

Through *in situ* SAXS study, they found that during the nucleation stage, particle growth was diffusion-limited (Figure 9b and c). In the transformation stage, growth was found to be limited by both reaction and diffusion, where the former was dominant. After the phase structure transformed into non-crystalline, diffusion-limited growth again dominated the particle growth.

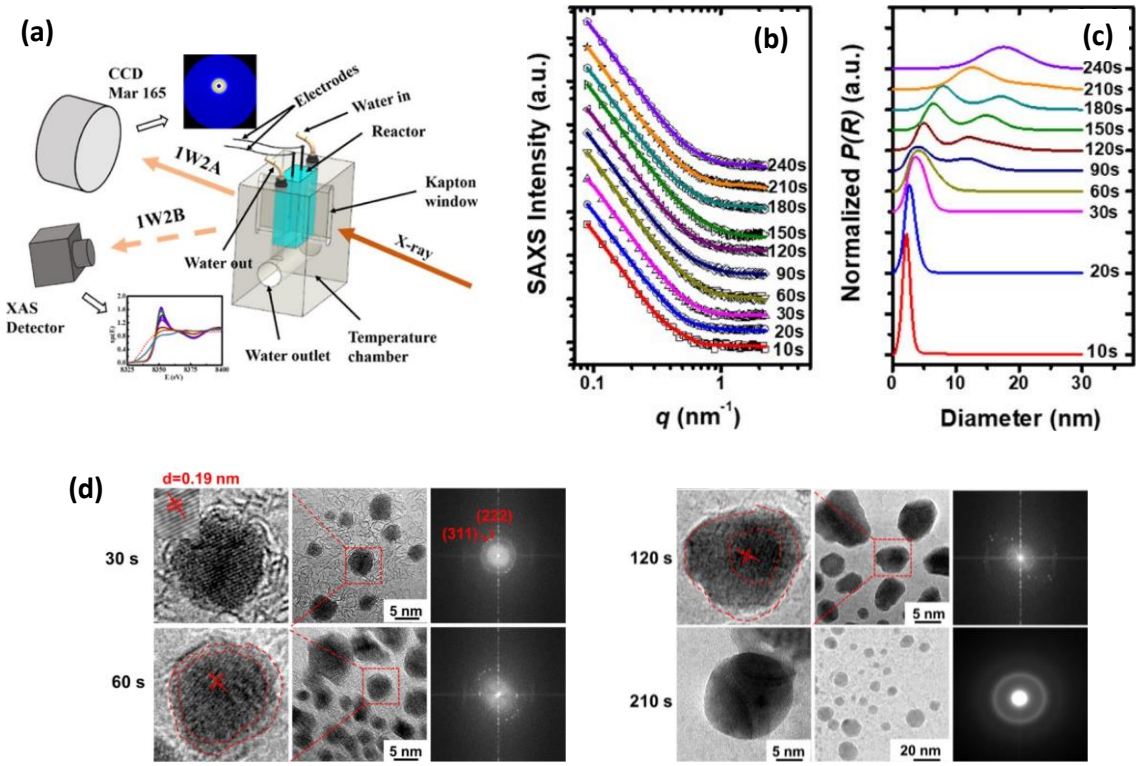

Figure 9 (a) Experimental setup of *in situ* XAFS and SAXS measurements on BSRF beamlines 1W2B and 1W2A. The Ni K-edge XAFS spectra were collected in transmission mode at a time interval of 30 s, while the SAXS patterns were recorded at a time interval of 10 s using a Mar 165 CCD detector. **(b)** Comparison between experimental SAXS intensities obtained during the formation of Ni-P NPs (symbols) and simulated SAXS intensities (solid lines) **(c)** Normalized particle volume distribution P(R) extracted from the SAXS data by the TBT method. (d) HRTEM images of the growing nanoparticles at reaction times of 30, 60, 120 and 210s, as indicated in the labels. Reprinted and adapted with permission from reference [67]. Copyright 2014, American Chemical Society.

Additionally, they collected samples at different reaction times and examined them using HRTEM (Figure 9d). The images provided valuable insights into the morphology and structural changes of the growing NPs over time. They observed that initially formed nanoparticles exhibited well-defined lattice fringes. As the reaction time increased, the size of the nanoparticles grew from approximately 3 to 15 nm. Concurrently, the lattice fringes at the nanoparticle edges became blurry, suggesting a transition from a crystalline to a non-crystalline phase structure. Ultimately, the nanoparticles completely transformed into a non-crystalline phase.

To gain a comprehensive understanding of the formation process *in situ* XAFS from both Ni and P edges was also employed. By combining the experimental results from all these techniques, the authors identified four main stages in the formation of the studied NPs: nucleation of crystalline Ni, nucleation of non-crystalline Ni-P, transformation from crystalline Ni to non-crystalline Ni-P, and further growth of the non-crystalline Ni-P NPs.

2.2.3 GISAXS/WAXS operando experiment

A very interesting example of the use of GISAXS combined with Grazing Incidence Wide Angle X-ray Scattering (GIWAXS) under *operando* conditions was presented by Martin and coworkers.[68] The work was focused on the study of periodically arranged and monodisperse Au NPs supported on flat silicon substrates that catalyze the hydrogenation of 1,3-butadiene. Importantly, the experiments were conducted under conditions that accurately mimic real-world working environments. A specialized gas flow reactor was used to expose 1 x 1 cm^2 supported Au NPs matrices on silicon to various gases at different temperatures. The reactor was connected to a custom-built gas supply system that included switching valves and mass flow controllers, allowing complete control of gas mixture and flow rates. In addition, the outlet was coupled to a mass spectrometer.

The authors analyzed 2D experimental and theoretical GISAXS patterns of Au NPs matrices during butadiene hydrogenation at 548 K (Figure 11c-d). The experimental pattern exhibited multiple peaks corresponding to (10), (11), (20), and (21) reflections of a two-dimensional hexagonal super lattice. The simulated pattern using the model presented in Figure 11a-b indicated the presence of four interference peaks in an idealized hexagonal lattice with the same lattice parameter and particle size distribution.

During butadiene hydrogenation, it was found that Au NPs are not inert but exist in a resting state before catalysis, characterized by the presence of a Au_2O_3 passivation layer (Figure 11g-i). The catalytically active state proves to be significantly different from the resting state. Specifically, reversible dynamism involving changes in size, shape, and phase was observed, with the height of the NPs increasing from 4.8 to 9.3 nm.

Reduced and fitted one-dimensional GISAXS profiles under various conditions showed a main interference peak at 0.095 nm^{-1}, corresponding to the hexagonal arrangement in the plane of Au NPs, as shown in Figure 11b. The fitted data revealed that this peak corresponded to a real-space distance of 76.3 nm, in excellent agreement with electron microscopy data. The intensity of higher-order peaks increased as the Au catalyst converted butadiene into but-1-enes and but-

2-enes, suggesting an increase in coherent scattering. These changes could be attributed to the NPs becoming more identical, resembling a reverse fusion effect.

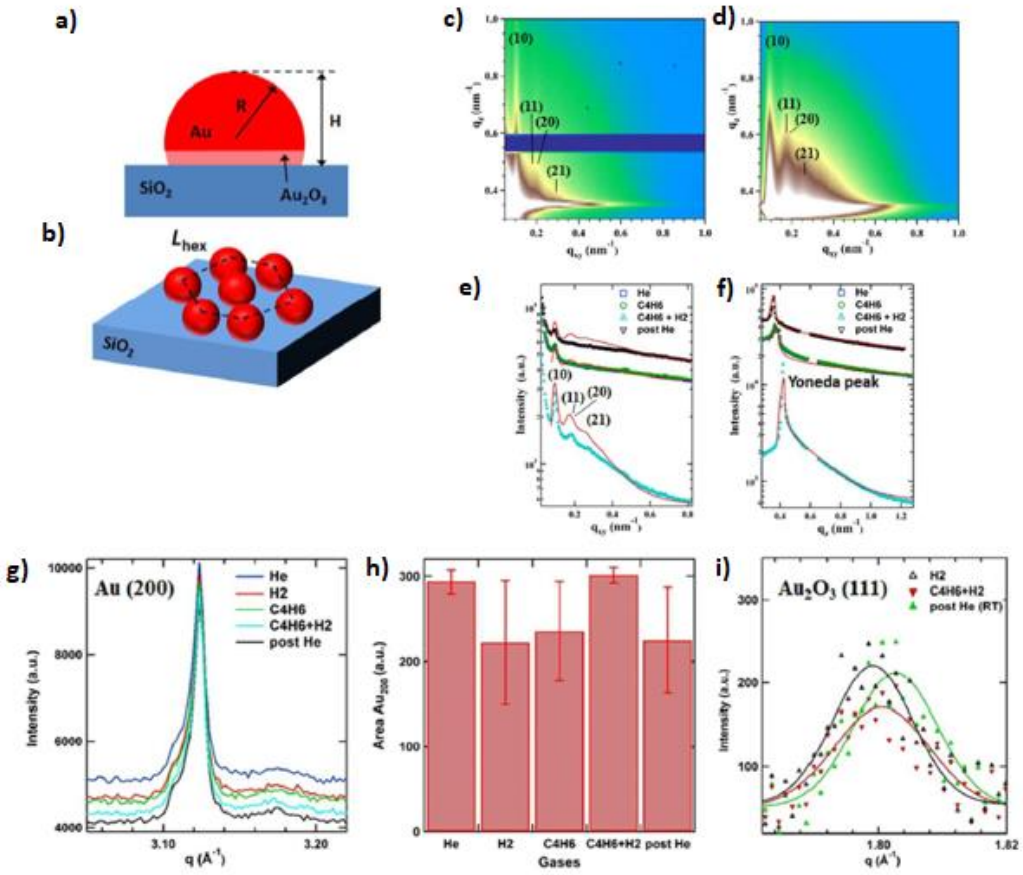

Figure 10 Schematic representation of the model used to fit the GISAXS data for the Au/SiO_2-Si catalysts: **(a)** spherical Au NP submerged in the SiO_2-Si(111) support, **(b)** Au NP hexagonal superlattice with the interparticle distance (L_{hex}) = 76.1 nm. Experimental **(c)** vs theoretical **(d)** 2D GISAXS images obtained during butadiene hydrogenation with the diffuse Kiessig fringes typical of NP monolayers with the narrow height distribution. **(e-f)** 1D GISAXS horizontal (q_z = 0.63 nm^{-1}) and vertical (q_{xy} = 0.16 nm^{-1}) experimental profiles (points) and corresponding fits (red lines) using IsGISAXS software of the supported Au NPs under various conditions. Changes in metallic Au content in the Au/SiO_2-Si catalyst during butadiene hydrogenation monitored by GIWAXS under *operando* conditions: **(g)** 1D GIWAXS profiles showing the (200) reflection of Au *fcc* lattice, **(h)** histograms showing calculated peak areas under various gas atmospheres, using a Voigt function for peak fitting and **(i)** 1D GIWAXS profiles of the (111) reflection of the Au_2O_3 crystal lattice. Reproduced from reference [68] with permission from the Royal Society of Chemistry.

This approach has great potential in identifying the actual active state of catalysts. For example, it could assist in designing highly reactive catalysts by exploring high aspect ratio and high surface energy forms, such as nanorods or other polyhedral shapes. Furthermore, the experimental setup used in this study could be expanded to monitor and investigate other important catalytic systems in the future, such as cobalt NPs for Fischer-Tropsch synthesis. Ultimately, this technique has the potential to become a valuable tool in the arsenal of catalysis researchers.

2.2.4 Quartz capillary Gases - SAXS

Another interesting example is the study of catalysts for the Fischer-Tropsch reaction, Kheres and collaborators have studied changes in the morphology of cobalt NPs catalysts by *in situ* SAXS measurements.[69] For this purpose, they have used the experimental scheme shown in Figure 11 a and b.

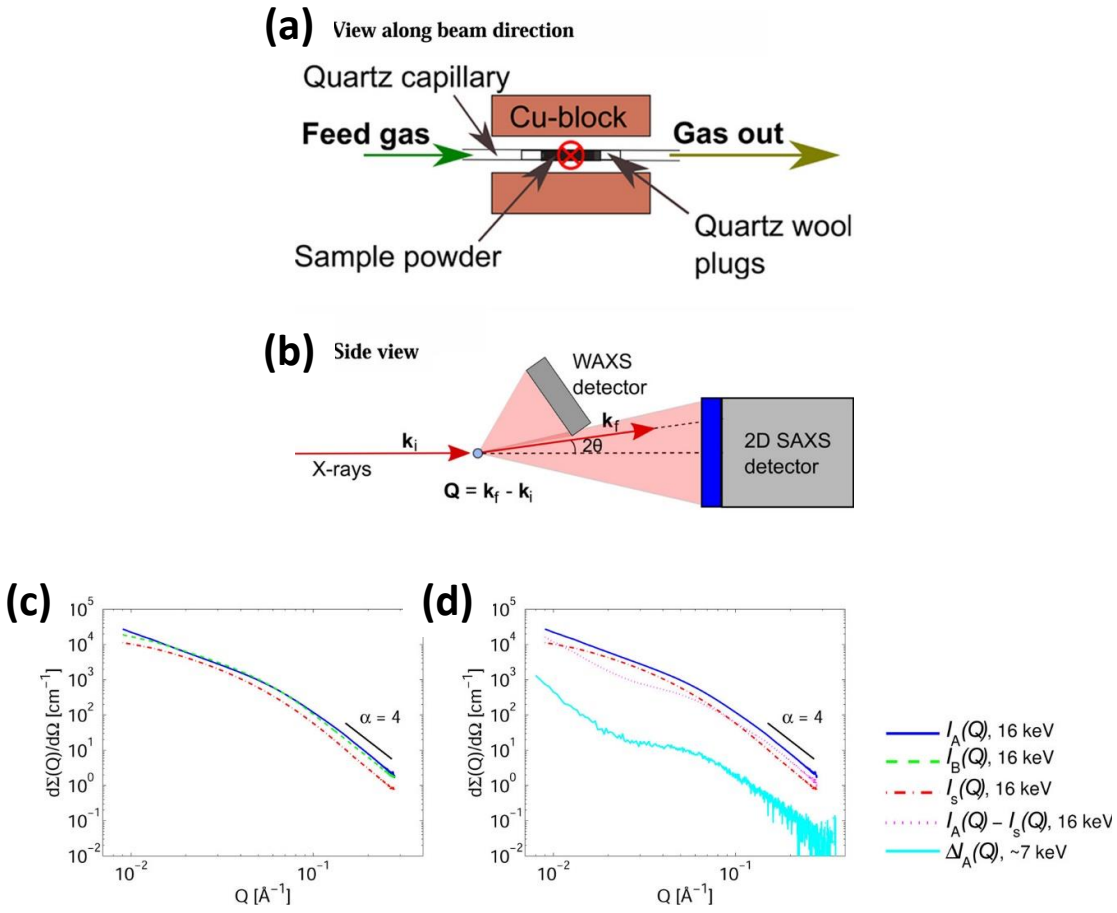

Figure 11. Scheme of experimental setup used to study catalysts for the Fischer-Tropsch reaction: **(a)** a quartz capillary containing the sample powder was mounted between Cu blocks for heating and connected to gas lines. The red cross indicates the X-Ray beam going into the paper plane. **(b)** Side-view of the SAXS and WAXS geometry. **(c)** SAXS patterns of two different samples (A and B) measured after reduction and the γ-alumina support ($I_S(Q)$), measured under ambient conditions (E = 16 keV). The black straight line indicates the Porod region where the power-law exponent α was found by fitting a straight line to the SAXS pattern. **(d)** $I_A(Q)$ and $I_S(Q)$ measured at E = 16 keV, and the difference between the two. The cyan curve is the ASAXS difference curve. Reprinted with permission from reference[69]. Copyright 2014, American Chemical Society.

By SAXS, Co NPs have been measured *in situ* for Fischer-Tropsch synthesis under practical catalytic conditions: input of H_2 and CO gases, heating to 210°C, pressure up to 10 bar, and support of γ-alumina. SAXS was employed to gain insights into the morphology of the particles during *in situ* experiments (Figure 11c-d). Additionally, simultaneous WAXS was utilized to track the reduction process of the oxide into catalytically active metal. Upon gas introduction, a notable increase in the slope of scattering intensity in the Porod region was observed, while the scattering invariant remained relatively constant. This finding suggests a modification in the shape or surface structure of the Co NPs. The experimental results were further analyzed, and different models explaining the observed shape and surface changes were discussed.

Small-angle scattering patterns were obtained for different samples after reduction, as shown in Figure 11c-d. However, due to the limited features observed in the curves, it is challenging to deduce a detailed structural model from the scattering data. The scattering curves exhibited a power-law slope in the high-Q region ($Q > 0.1$ Å^{-1}) and a weak shoulder in the region 0.04 Å$^{-1} < Q < 0.07$ Å^{-1}. The position of the shoulder is related to the radii of gyration of the scattering objects. In this case, the shoulder was hardly observable due to the overlapping signals from polydisperse cobalt particles and the irregular pore structure of the alumina support. The size distributions of the different constituents were highly polydisperse and overlapping, making it difficult to determine a unique solution for the actual size distributions. Hence, a model-independent analysis based on SAXS was employed in this study. Additional measurements were conducted using ASAXS around the Co K-edge to better separate the contributions of the Co NPs to the scattering signal (Figure 11d).

Overall, the work describes the challenges in determining a detailed structural model from SAXS data and highlights the significance of the observed scattering features in understanding the behavior of cobalt particles and alumina support in the catalytic system under investigation.[69]

2.2.5 Quartz capillary-Multi techniques SAXS-WAXS-UV-Vis

Another sample environment is the flow cell, which in turn can be combined with other techniques. For example, Förster and coworkers used the experimental setup schematized in Figure 12a to study the nucleation and growth of Au NPs as a function of different experimental parameters: temperature, concentration and solvents.[70] Au NPs are widely used as catalyst either supported or in solution and the study of their formation process results fundamental in the catalysis field.[71]

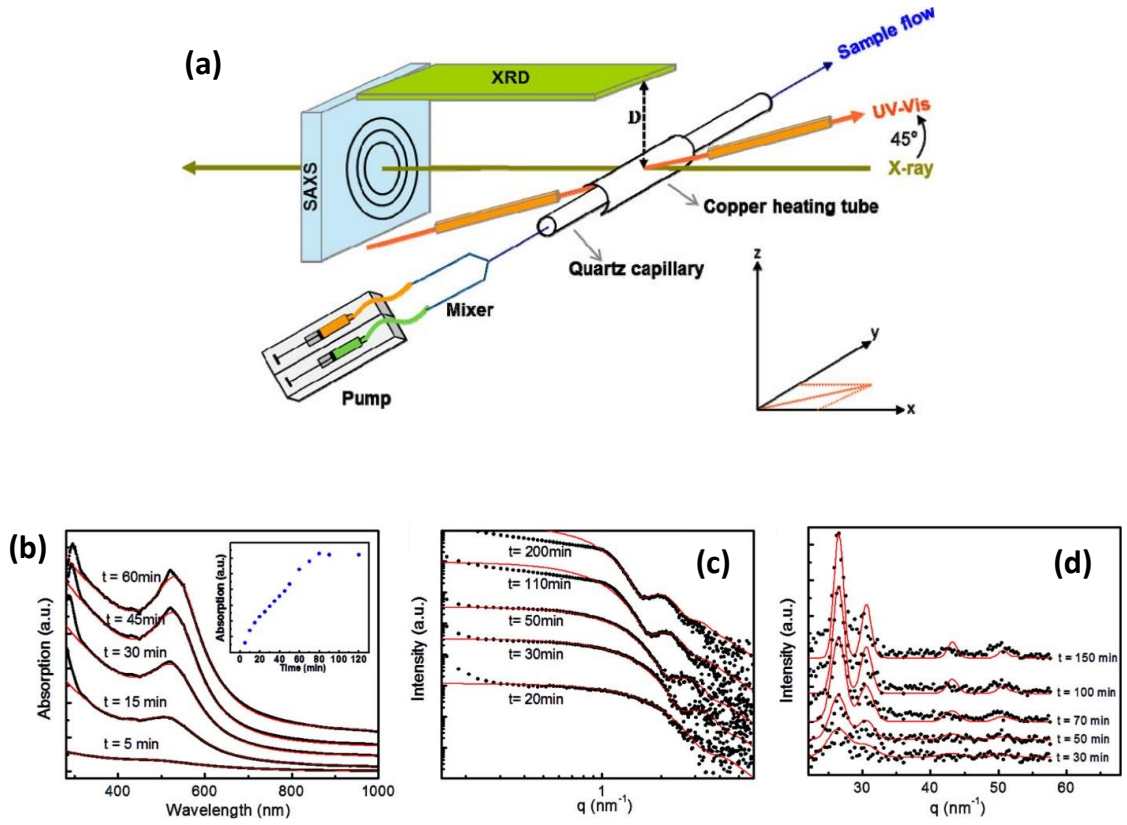

Figure 12 (a) Experimental setup for in situ SAXS/WAXS/UV–Vis measurements of formation of Au NPs. Characteristic **(b)** UV/Vis-spectra, **(c)** SAXS curves, and **(d)** WAXS curves measured at different times during the nucleation and growth of the Au NPs together with the corresponding fits (solid lines) for quantitative analysis. The inset in (b) is the intensity of plasmon resonance band versus reaction time. Reprinted with permission from reference [70]. Copyright 2015, American Chemical Society.

Figure 12c illustrates the SAXS scattering curves obtained during the experiment, providing valuable insights into the NPs formation process. Within the first 30 minutes, a Guinier-plateau was observed in the 0.4 nm^{-1} < q < 1.0 nm^{-1} range, indicating the formation of small NPs with a radius below 1.5 nm. A small low-q upturn for q < 0.4 nm^{-1} was also observed, suggesting the presence of larger aggregates of unknown structure. As time progressed, a pronounced form factor oscillation was observed, indicating the growth of monodisperse NPs, which was further supported by the appearance and red-shift of a sharp plasmon peak in the UV-Vis spectra (Figure 12b). The Guinier plateau also exhibited a shallow slope as time increased, indicating the formation of nanoparticle assemblies.

In situ WAXS measurements, on the other hand, provided information about the crystalline nature of the Au NPs during the formation process: the appearance and growth of two strong diffraction peaks was observed as the reaction proceed (Figure 12d). Interestingly, the intensity of the (111) peak increased over time, while the full-width at half-maximum decreased, indicating a continuous increase in the crystalline domain size during NPs growth.

Overall, these observations provided valuable information about the size, structure, and crystallinity of the formed Au NPs during the experimental process. Remarkably, from these results the authors were able were able to fit nucleation and growth models based on comparing the time evolution of radius, polydispersity and number of NPs.

In summary, it is clear that *in situ* and *operando* studies of catalytic processes under conditions closer to operational ones help to understand the fundamentals and processes that occur in catalysts and gives great input on how to improve their activity.

3) Summary and Outlook

Along this review, we showed that SAS techniques can provide very useful information about structure of catalysts at the nanoscale and how this affects the catalytic processes. Insight from these techniques combined with other tools help to complete this picture, making room for improving their performance or opening new alternatives for both catalysts synthesis and use.

We have presented several examples of experiments performed *ex situ* that provide key information about catalyst preparation, including information about particles characteristics, and pore arrangement, among other features. Moreover, we showed that SAS experiments shed light on how the active nanoparticles are distributed within solid supports, an important condition for modelling diffusion/reactions chemical mechanisms that occur within these catalysts. *In situ* and *operando* experiments, on the other hand, provide fundamental

information about the behaviour of catalysts under operational or close to operational conditions. Some examples were presented about the potentiality of this approach and the possibility of combining SAS with other characterization techniques. Interestingly, we noted that performing *ex situ* characterization of catalysts before and after their use, although simpler than *in situ* or *operando* approaches, is not a common practice in the catalysis field.

SAXS is the most used SAS technique for the study of catalysts, either alone or combined with other X-Ray based methods. This fact can be explained considering that SAXS instruments are far more accessible, due to the availability of a wide variety of laboratory equipment and as X-ray sources are simpler to fabricate. Moreover, worldwide there is a considerable number of X-ray synchrotron facilities with bright sources. In contrast, although it presents a huge potential thanks to the differential characteristics of neutrons in comparison with X-Rays, SANS examples on catalytic applications are scarce. This fact can be ascribed to the proper limitations of the technique due to the following reasons: i) the much smaller quantity of available instruments worldwide as neutrons are delivered using nuclear reactions in reactors and accelerators, demanding special licensing and ii) longer times required to acquire information due to limited temporal resolution. In this sense, we highlight that South America and the rest of the world will soon have access to two state of the art SANS beamlines in the *Laboratorio Argentino de Haces de Neutrones* (Neutron Beams Argentinean Laboratory, LAHN), currently being built in Argentina by the Comisión Nacional de Energía Atómica (CNEA). LAHN is aimed for the study and characterization of materials with state-of-the-art neutron techniques, making use of neutron beams provided by the RA-10 reactor, also under construction.

In summary, the advantages of SAS techniques open up an exciting road for catalysts development. Shortcomings, on the other hand, challenge the scientist community to look out for innovative solutions. However, the perspectives are reassuring as synchrotron radiation is more accessible and neutron radiation sources are growing with a “spilling -over” effect on the available techniques for materials characterization and processes studies.

Acknowledgements

This work was supported by Agencia I+D+i (PICT 2019-01615). Dr. Gustavo Segovia is gratefully acknowledged for his help in Figure 1 preparation.

Keywords

Heterogeneous catalysis; Materials science; Mesoporous materials; Nanoparticles; Small Angle Neutron Scattering; Small Angle X Ray Scattering; Supported catalysts.

Conflict of Interest statement

The authors do not have any conflict of interest to declare

References

[1] N. Pal, A. Bhaumik, *RSC Advances* **2015**, *5*, 24363-24391.

[2] aA. Taguchi, F. Schüth, *Microporous Mesoporous Mater.* **2005**, *77*, 1-45; bD. Astruc, *Chem. Rev.* **2020**, *120*, 461-463.

[3] A. Sápi, T. Rajkumar, J. Kiss, Á. Kukovecz, Z. Kónya, G. A. Somorjai, *Catal. Lett.* **2021**, *151*, 2153-2175.

[4] aJ. Liang, Z. Liang, R. Zou, Y. Zhao, *Adv. Mater.* **2017**, *29*, 1701139; bB. Louis, G. Laugel, P. Pale, M. M. Pereira, *ChemCatChem* **2011**, *3*, 1263-1272; cY.-Z. Chen, R. Zhang, L. Jiao, H.-L. Jiang, *Coord. Chem. Rev.* **2018**, *362*, 1-23; dJ. Čejka, S. Mintova, *Catalysis Reviews* **2007**, *49*, 457-509; eX. Xu, S. K. Megarajan, Y. Zhang, H. Jiang, *Chem. Mater.* **2020**, *32*, 3-26.

[5] aE. Cortés, L. V. Besteiro, A. Alabastri, A. Baldi, G. Tagliabue, A. Demetriadou, P. Narang, *ACS Nano* **2020**, *14*, 16202-16219; bK. An, G. A. Somorjai, *ChemCatChem* **2012**, *4*, 1512-1524.

[6] R. Ciriminna, E. Falletta, C. Della Pina, J. H. Teles, M. Pagliaro, *Angew. Chem. Int. Ed.* **2016**, *55*, 14210-14217.

[7] aJ. Haber, J. H. Block, B. Delmon, in *Handbook of Heterogeneous Catalysis* (Eds.: G. Ertl, H. Knözinger, F. Schüth, J. Weitkamp), **2008**, pp. 1230-1258; bN. E. Tsakoumis, A. P. E. York, D. Chen, M. Rønning, *Catal. Sci. Technol.* **2015**, *5*, 4859-4883; cI. P. Silverwood, S. F. Parker, C. R. A. Catlow, *Physical Chemistry Chemical Physics* **2016**, *18*, 17140-17140; dZ. Wu, A. J. Ramirez-Cuesta, K. Fukutani, *Top. Catal.* **2021**, *64*, 591-592; e*Characterization of Solid Materials and Heterogeneous Catalysts: From Structure to Surface Reactivity*, **2012**.

[8] aM. Behrens, R. Schlögl, in *Characterization of Solid Materials and Heterogeneous Catalysts*, **2012**, pp. 609-653; bC. J. Gommes, S. Jaksch, H. Frielinghaus, *J. Appl. Crystallog.* **2021**, *54*, 1832-1843; cH. Jobic, in *Characterization of Solid Materials and Heterogeneous Catalysts*, **2012**, pp. 185-209.

[9] aR.-J. Roe, *Methods of X-ray and neutron scattering in polymer science*, Oxford University Press, **2000**; bY. B. Melnichenko, in *Small-Angle Scattering from Confined and Interfacial Fluids: Applications to Energy Storage and Environmental Science* (Ed.: Y. B. Melnichenko), Springer International Publishing, Cham, **2016**, pp. 1-18.

[10] X. Zuo, B. Lee, in *Encyclopedia of Nanomaterials (First Edition)* (Eds.: Y. Yin, Y. Lu, Y. Xia), Elsevier, Oxford, **2023**, pp. 13-38.

[11] J. Teixeira, *J. Appl. Crystallogr.* **1988**, *21*, 781-785.

[12] P. Müller-Buschbaum, *Polym J* **2013**, *45*, 34-42.

[13] J. S. Pedersen, in *Modern Aspects of Small-Angle Scattering* (Ed.: H. Brumberger), Springer Netherlands, Dordrecht, **1995**, pp. 57-91.

[14] V. F. Sears, *Neutron News* **1992**, *3*, 26-37.

[15] T. Zhao, X. Huang, R. Cui, W. Han, G. Zhang, Z. Tang, *Journal of Cleaner Production* **2023**, 136125.

[16] aY. Zhou, Y. Li, Y. Hou, C. Wang, Y. Yang, J. Shang, X. Cheng, *Chemical Engineering Journal* **2022**, 140604; bC. J. Gommes, G. Prieto, P. E. De Jongh, *J. Phys. Chem. C* **2016**, *120*, 1488-1506.

[17] Y. Li, Y. Wu, K. Liu, S. A. Delbari, A. Kim, A. Sabahi Namini, Q. V. Le, M. Shokouhimehr, C. Xia, H. W. Jang, R. S. Varma, R. Luque, *Fuel* **2023**, *340*, 127482.

[18] S. Ding, K. Motokura, *Current Opinion in Green and Sustainable Chemistry* **2023**, 100753.

[19] B. Ingham, *Crystallogr Rev* **2015**, *21*, 229-303.

[20] aS. Bhunia, D. Saha, S. Koner, *Langmuir* **2011**, *27*, 15322-15329; bA. Fischereder, M. L. Martinez-Ricci, A. Wolosiuk, W. Haas, F. Hofer, G. Trimmel, G. J. A. A. Soler-Illia, *Chemistry of Materials* **2012**, *24*, 1837-1845; cI. Tamiolakis, I. N. Lykakis, A. P. Katsoulidis, C. D. Malliakas, G. S. Armatas, *J. Mater. Chem.* **2012**, *22*, 6919-6927; dS. Böttcher, C. Hoffmann, K. Räuchle, W. Reschetilowski, *ChemCatChem* **2011**, *3*, 741-748.

[21] aC. Yang, J. H. Meldon, B. Lee, H. Yi, *Catalysis Today* **2014**, *233*, 108-116; bS. Kabir, D. J. Myers, N. Kariuki, J. Park, G. Wang, A. Baker, N. Macauley, R. Mukundan, K. L. More, K. C. Neyerlin, *ACS Appl. Mater. Interfaces* **2019**.

[22] G. J. A. A. Soler-Illia, C. Sanchez, B. Lebeau, J. Patarin, *Chem. Rev.* **2002**, *102*, 4093-4138.

[23] M. J. Hollamby, *Physical Chemistry Chemical Physics* **2013**, *15*, 10566-10579.

[24] H. A. Beejapur, V. La Parola, L. F. Liotta, M. L. Testa, *ChemistrySelect* **2017**, *2*, 4934-4941.

[25] C. Xiao, R. V. Maligal-Ganesh, T. Li, Z. Qi, Z. Guo, K. T. Brashler, S. Goes, X. Li, T. W. Goh, R. E. Winans, W. Huang, *ChemSusChem* **2013**, *6*, 1915-1922.

[26] B. Tan, S. E. Rankin, *The Journal of Physical Chemistry B* **2004**, *108*, 20122-20129.

[27] H. Gustafsson, C. Thörn, K. Holmberg, *Colloids Surf. B Biointerfaces* **2011**, *87*, 464-471.

[28] R. Maheswari, M. P. Pachamuthu, A. Ramanathan, B. Subramaniam, *Ind. Eng. Chem. Res.* **2014**, *53*, 18833-18839.

[29] B. Castanheira, L. Otubo, C. L. P. Oliveira, R. Montes, J. B. Quintana, R. Rodil, S. Brochsztain, V. J. P. Vilar, A. C. S. C. Teixeira, *Chemosphere* **2022**, *287*.

[30] W. Janssens, E. V. Makshina, P. Vanelderen, F. De Clippel, K. Houthoofd, S. Kerkhofs, J. A. Martens, P. A. Jacobs, B. F. Sels, *ChemSusChem* **2015**, *8*, 994-1008.

[31] aK. Khan, Z. N. Siddiqui, *Monatsh. Chem.* **2015**, *146*, 2097-2105; bJ. O. Damas, S. B. Moscardini, L. R. Oliveira, R. R. da Silva, E. J. Nassar, E. H. de Faria, K. J. Ciuffi, S. J. L. Ribeiro, L. A. Rocha, *Mater Chem Phys* **2019**, *225*, 145-152; cD. M. Morales, R. A. Frenzel, G. P. Romanelli, L. R. Pizzio, *Mol. Cat.* **2020**, *481*; dS. Rahman, S. Shah, C. Santra, D. Sen, S. Sharma, J. K. Pandey, S. Mazumder, B. Chowdhury, *Microporous Mesoporous Mater.* **2016**, *226*, 169-178.

[32] B. Gouze, J. Cambedouzou, S. Parrès-Maynadié, D. Rébiscoul, *Microporous Mesoporous Mater.* **2014**, *183*, 168-176.

[33] C. J. Gommes, G. Prieto, J. Zecevic, M. Vanhalle, B. Goderis, K. P. DeJong, P. E. DeJongh, *Angew. Chem. Int. Ed.* **2015**, *54*, 11804-11808.

[34] J. Radnik, T. T. H. Dang, S. Gatla, V. S. Raghuwanshi, D. Tatchev, A. Hoell, *RSC Adv.* **2019**, *9*, 6429-6437.

[35] aS. Bakardjieva, R. Fajgar, I. Jakubec, E. Koci, A. Zhigunov, E. Chatzisymeon, K. Davididou, *Catalysis Today* **2019**, *328*, 189-201; bP. Z. Araujo, V. Luca, P. B. Bozzano, H. L. Bianchi, G. J. d. Á. A. Soler-Illia, M. A. Blesa, *ACS Applied Materials & Interfaces* **2010**, *2*, 1663-1673.

[36] S. Cao, Y. Sun, Y. Shang, J. Wang, Y. Gong, G. Mo, Z. Li, Z. D. Zhang, A. Ma, *Mol. Cat.* **2022**, *524*.

[37] J. Xu, T. Chen, J. K. Shang, K. Z. Long, Y. X. Li, *Microporous Mesoporous Mater.* **2015**, *211*, 105-112.

[38] A. K. Ilunga, B. B. Mamba, T. T. I. Nkambule, *Appl. Organomet. Chem.* **2021**, *35*.

[39] M. C. Orilall, F. Matsumoto, Q. Zhou, H. Sai, H. D. Abruña, F. J. DiSalvo, U. Wiesner, *J. Am. Chem. Soc.* **2009**, *131*, 9389-9395.

[40] M. Burton, A. Selvam, J. Lawrie-Ashton, A. Squires, N. Terrill, I. Nandhakumar, *ACS Appl. Mater. Interfaces* **2018**, *10*, 37087-37094.

[41] E. A. Franceschini, G. A. Planes, F. J. Williams, G. J. A. A. Soler-Illia, H. R. Corti, *Journal of Power Sources* **2011**, *196*, 1723-1729.

[42] A. Forgács, Z. Balogh, M. Andrási, A. Len, Z. Dudás, N. V. May, P. Herman, L. Juhász, I. Fábián, N. Lihi, J. Kalmár, *Appl Surf Sci* **2022**, *579*.

[43] S. Rahman, C. Santra, R. Kumar, J. Bahadur, A. Sultana, R. Schweins, D. Sen, S. Maity, S. Mazumdar, B. Chowdhury, *Appl Catal A Gen* **2014**, *482*, 61-68.

[44] R. Kumar, S. Shah, J. Bahadur, Y. B. Melnichenko, D. Sen, S. Mazumder, C. P. Vinod, B. Chowdhury, *Microporous Mesoporous Mater.* **2016**, *234*, 293-302.

[45] F. Chabot, J. Lee, F. Vandenberghe, L. Guétaz, G. Gebel, S. Lyonnard, L. Porcar, S. Rosini, A. Morin, *ACS Appl. Ener. Mat.* **2023**, *6*, 1185-1196.

[46] aJ. Tian, Z. Y. Xu, D. W. Zhang, H. Wang, S. H. Xie, D. W. Xu, Y. H. Ren, H. Wang, Y. Liu, Z. T. Li, *Nat. Commun.* **2016**, *7*, 11580 ; bY. C. Zhang, Z. Y. Xu, Z. K. Wang, H. Wang, D. W. Zhang, Y. Liu, Z. T. Li, *ChemPlusChem* **2020**, *85*, 1498-1503; cJ. Mor, S. K. Sharma, P. Utpalla, J. Bahadur, J. Prakash, A. Kumar, P. K. Pujari, *Microporous Mesoporous Mater.* **2022**, *335*.

[47] T. Li, A. J. Senesi, B. Lee, *Chem. Rev.* **2016**, *116*, 11128-11180.

[48] M. Heilmann, C. Prinz, R. Bienert, R. Wendt, B. Kunkel, J. Radnik, A. Hoell, S. Wohlrab, A. Guilherme Buzanich, F. Emmerling, *Adv. Eng. Mater.* **2022**, *24*.

[49] H. Wang, G. Lin, X. Li, W. Lu, Z. Peng, *J. Colloid Interface Sci.* **2019**, *554*, 396-403.

[50] J. Kronawitt, M. Dulle, H. Schmalz, S. Agarwal, A. Greiner, *ACS Appl. Nano Mat.* **2020**, *3*, 2766-2773.

[51] S. C. Buratto, E. Latocheski, D. C. de Oliveira, J. B. Domingos, *J. Braz. Chem. Soc.* **2020**, *31*, 1078-1085.

[52] P. E. J. Saloga, T. Rybak, A. F. Thünemann, *Adv. Eng. Mater.* **2022**, *24*.

[53] A. I. Trypolskyi, T. M. Gurnyk, P. E. Strizhak, *Catal. Commun.* **2011**, *12*, 766-771.

[54] D. A. Kozlov, A. B. Shcherbakov, T. O. Kozlova, B. Angelov, G. P. Kopitsa, A. V. Garshev, A. E. Baranchikov, O. S. Ivanova, V. K. Ivanov, *Molecules* **2020**, *25*.

[55] M. Duss, J. J. Vallooran, L. Salvati Manni, N. Kieliger, S. Handschin, R. Mezzenga, H. J. Jessen, E. M. Landau, *Langmuir* **2019**, *35*, 120-127.

[56] J. Quinson, M. Inaba, S. Neumann, A. A. Swane, J. Bucher, S. B. Simonsen, L. Theil Kuhn, J. J. K. Kirkensgaard, K. M. Jensen, M. Oezaslan, S. Kunz, M. Arenz, *ACS Catal.* **2018**, *8*, 6627-6635.

[57] M. O'Neill, V. S. Raghuwanshi, R. Wendt, M. Wollgarten, A. Hoell, K. Rademann, *Z. Phys. Chem.* **2015**, *229*, 221-234.

[58] aW. Yoshimune, M. Harada, in *ECS Transactions, Vol. 98*, 9 ed., **2020**, pp. 447-454; bS. Koizumi, S. Ueda, T. Inada, Y. Noda, R. A. Robinson, *J. Appl. Crystallog.* **2019**; cW. Yoshimune, M. Harada, *Chem. Lett.* **2019**, *48*, 487-490; dT. Kusano, T. Hiroi, K. Amemiya, M. Ando, T. Takahashi, M. Shibayama, *Polym J* **2015**, *47*, 546-555; eM. Shibayama, T. Matsunaga, T. Kusano, K. Amemiya, N. Kobayashi, T. Yoshida, *J. Appl. Polym. Sci.* **2014**, *131*; fA. Ghedjatti, N. Coutard, L. Calvillo, G. Granozzi, B. Reuillard, V. Artero, L. Guetaz, S. Lyonnard, H. Okuno, P. Chenevier, *Chem. Sci.* **2021**, *12*, 15916-15927.

[59] M. Staropoli, D. Gerstner, A. Radulescu, M. Sztucki, B. Duez, S. Westermann, D. Lenoble, W. Pyckhout-Hintzen, *Polym.* **2020**, *12*.

[60] S. H. Kim, S. Han, H. Ha, J. Y. Byun, M. H. Kim, *Catalysis Today* **2016**, *260*, 46-54.

[61] S. Bjelić, U. Gasser, I. Alxneit, F. Vogel, *ChemCatChem* **2019**, *11*, 1747-1755.

[62] J. Dendooven, R. K. Ramachandran, E. Solano, M. Kurttepeli, L. Geerts, G. Heremans, J. Rongé, M. M. Minjauw, T. Dobbelaere, K. Devloo-Casier, J. A. Martens, A. Vantomme, S. Bals, G. Portale, A. Coati, C. Detavernier, *Nat. Commun.* **2017**, *8*.

[63] I. L. Violi, M. D. Perez, M. C. Fuertes, G. J. A. A. Soler-Illia, *ACS Appl. Mater. Interfaces* **2012**, *4*, 4320-4330.

[64] I. L. Violi, A. Zelcer, M. M. Bruno, V. Luca, G. J. A. A. Soler-Illia, *ACS Appl. Mater. Interfaces* **2015**, *7*, 1114-1121.
[65] aJ. Feng, M. Kriechbaum, L. Liu, *Nanotechnology Reviews* **2019**, *8*, 352-369; bE. K. Gibson, I. P. Silverwood, P. P. Wells, S. F. Parker, in *Modern Developments in Catalysis*, **2017**, pp. 41-88; cW. Bras, S. Koizumi, N. J. Terrill, *IUCrJ* **2014**, *1*, 478-491.
[66] S. Ueda, S. Koizumi, A. Ohira, S. Kuroda, H. Frielinghaus, *Physica B: Condensed Matter* **2018**, *551*, 309-314.
[67] Y. Tan, D. Sun, H. Yu, S. Jiao, Y. Gong, S. Yan, Z. Chen, X. Xing, G. Mo, Q. Cai, Z. Wu, *J. Phys. Chem. C* **2018**, *122*, 16397-16405.
[68] D. J. Martin, D. Decarolis, Y. I. Odarchenko, J. J. Herbert, T. Arnold, J. Rawle, C. Nicklin, H.-G. Boyen, A. M. Beale, *Chemical Communications* **2017**, *53*, 5159-5162.
[69] K. Høydalsvik, J. B. Fløystad, A. Voronov, G. J. B. Voss, M. Esmaeili, J. Kehres, H. Granlund, U. Vainio, J. W. Andreasen, M. Rønning, D. W. Breiby, *J. Phys. Chem. C* **2014**, *118*, 2399-2407.
[70] X. Chen, J. Schröder, S. Hauschild, S. Rosenfeldt, M. Dulle, S. Förster, *Langmuir* **2015**, *31*, 11678-11691.
[71] D. Astruc, F. Lu, J. R. Aranzaes, *Angew. Chem. Int. Ed.* **2005**, *44*, 7852-7872.

10.1002/cctc.202300490

Table of Contents

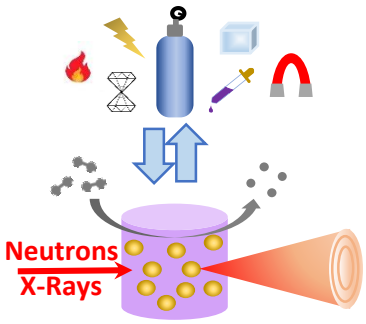

The main aspects of the use of Small Angle Scattering based techniques are reviewed in this work. The main characteristics of X-Ray and neutrons based techniques are discussed. Examples about the characterization of several catalysts families before, during and after catalytic reactions are presented and discussed.

10.1002/cctc.202300490

Frontispiece

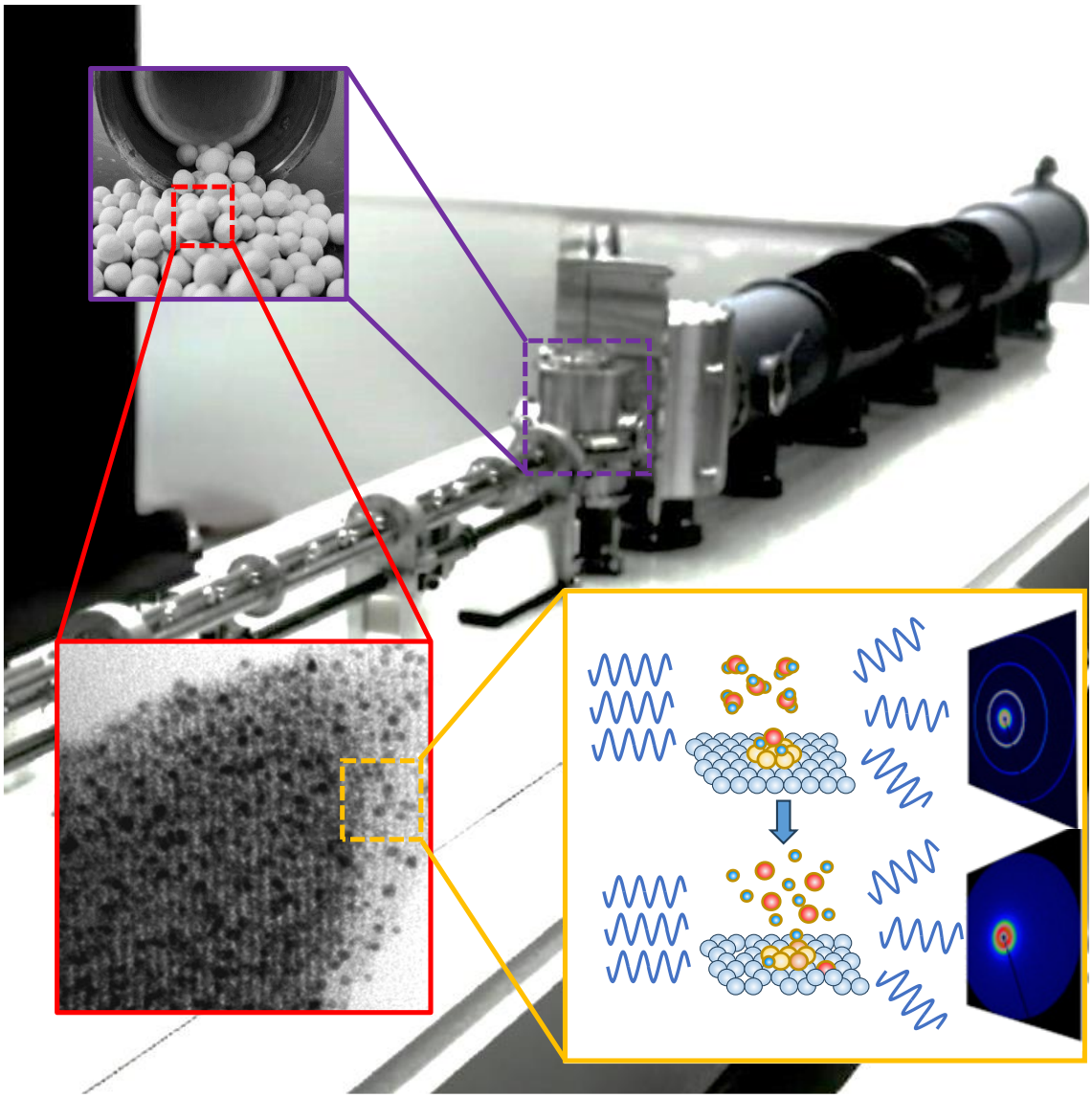

10.1002/cctc.202300490

Twitter users

Facundo Herrera @Facu_Herrera

Paula C. Angelomé @pcangelome

Biographies

Facundo Herrera has a degree in Physics from UNICEN and a PhD in Exact Sciences: Physics Area from UNLP, Argentina. His thesis was based on the development of the controlled generation of nanostructured surfaces with extended order, under the direction of Prof. Requejo. He then carried out postdoctoral studies in several Institutes: INIFTA-UNLP (La Plata, Argentina), NAPP-XPS CIRCE line at ALBA Synchrotron (Spain), GET laboratory of the Paul Sabatier University (France), Institute of Nanosystems UNSAM and Comisión Nacional de Energía Atómica, where he is currently developing as a researcher to work on the implementation of SANS techniques and sample environments.

Gonzalo A. Rumi received his undergraduate degree in physics from the Universidad Nacional de La Plata (2015), and his PhD from Instituto Balseiro (2020), in Argentina. His main interests lie in the development and application of neutron-based techniques for characterization of condensed matter systems. In particular, he is interested in Small-Angle Neutron Scattering for the study of mesoporous oxides and vortex matter in superconductors. He is currently working at the Argentinean Neutron Beam Laboratory (LAHN), in close collaboration with the Chemistry of Nanomaterials Group for the implementation of SANS techniques in Argentina.

Paula Y. Steinberg got her degree in chemistry in 2010 and her PhD in chemistry in 2018, both at the Universidad de Buenos Aires, Argentina. Her PhD thesis concerned the study of the structural control of TiO_2 mesoporous thin films and its effects on the transport and reactivity within confined environments. She worked as a postdoctoral fellow at the Physicochemical of Fluids group (CAC, CNEA) with Drs. Japas and Mirenda (2019-2022). Since 2022, she is a researcher at LAHN, CNEA. Her current main interests include the study of luminescent ionic liquids and the use of SAXS and SANS to characterize their nanostructures.

Alejandro Wolosiuk is a BS and PhD in Chemistry (UBA, Argentina). He carried on a postdoctoral stay at the University of Illinois at Urbana-Champaign (Department of Materials Science and Engineering). Since 2006, he is a research fellow of CONICET and Comisión Nacional de Energía Atómica (CNEA). His research interests include the synthesis of colloids and nanoparticles, the study of their interfaces and how to integrate diverse chemical building blocks for designing nanoobjects aimed for adsorption and sensing.

Paula C. Angelomé has a Degree (2003) and a PhD (2008) in Chemistry, both from Universidad de Buenos Aires, Argentina. During her thesis, she developed methods to obtain hybrid and pure oxide mesoporous thin films. Between 2008 and 2012, she was a postdoctoral fellow at Universidade de Vigo (Spain), where she worked on metallic nanoparticles synthesis and characterization. Since 2012, she is a CONICET researcher at CAC-CNEA, Argentina. Her current main interests are the design, synthesis and exhaustive characterization of materials based on mesoporous thin films and metallic nanoparticles and the study of their applications in catalysis and sensing.